

Quantum interference in the resonance fluorescence of a $J = 1/2 - J' = 1/2$ atomic system: Quantum beats, nonclassicality, and non-Gaussianity

H. M. Castro-Beltrán,^{1,*} O. de los Santos-Sánchez,² L. Gutiérrez,³ and A. D. Alcantar-Vidal¹

¹*Centro de Investigación en Ingeniería y Ciencias Aplicadas and Instituto de Investigación en Ciencias Básicas y Aplicadas, Universidad Autónoma del Estado de Morelos, Avenida Universidad 1001, 62209 Cuernavaca, Morelos, México*

²*Tecnologico de Monterrey, Escuela de Ingeniería y Ciencias, Ave. Carlos Lazo 100, Santa Fe, Mexico City, Mexico, 01389*

³*Instituto de Ciencias Físicas, Universidad Nacional Autónoma de México, 62210 Cuernavaca, Morelos, México*

(Dated: January 10, 2023)

We study the resonance fluorescence of a system with angular momentum $J = 1/2 - J' = 1/2$ level structure driven by a single, linearly polarized, monochromatic laser field. Quantum interference among the two, antiparallel, π transitions leads to rich results. We develop the article around two broad overlapping themes: (i) the observation of quantum beats in the intensity and the dipole-dipole, intensity-intensity, and quadrature-intensity correlations, when the atom is subject to a strong laser and large Zeeman splittings. The mean and modulation frequencies of the beats are given by the average and difference, respectively, among two close generalized Rabi frequencies related to a Mollow-like spectrum with two pairs of sidebands. (ii) The nonclassical and non-Gaussian properties of phase-dependent fluorescence for the cases of weak to moderate excitation and in the regime of beats. The fluorescence in the beats regime is nonclassical, mainly from the third-order dipole fluctuations, which reveal them to be also strongly non-Gaussian. For weak to moderate driving laser and small detunings and Zeeman splittings the nonclassicality is an interplay of second- (squeezing) and third-order dipole noise.

I. INTRODUCTION

Recently, the properties of the resonance fluorescence of a single atomic system with angular momentum transition $J = 1/2 - J' = 1/2$ driven by a monochromatic laser have been the subject of great interest due to the possibility of observing vacuum-induced coherence effects due to interference among the two antiparallel π transitions, emitting into the same frequency range of the electromagnetic vacuum. Here, the π transitions are incoherently coupled, mediated by spontaneous emission in the σ transitions and then excited by the laser. The antiparallel dipoles of the transitions makes it realistic to observe interference effects, while V and Λ three-level systems require additional preparation because the transitions are perpendicular [1, 2]. Particular attention has been devoted to the spectrum [3–6], time-energy complementarity [4, 5], Young’s interference [7], photon correlations [8], frequency-resolved photon correlations [9], squeezing [10], phase shifts [11], and cooperative effects in photon correlations [12]. The case of additional laser excitation of one of the σ transitions on the spectrum and squeezing has been studied in [13–15].

Quantum beats are among the more familiar manifestations of quantum interference. They appear in the modulation of the decay by spontaneous emission of multilevel systems due to the energy difference among transitions [2]. So far, few experiments of quantum interference experiments have been performed on the $J = 1/2 - J' =$

$1/2$, in this case observing Young-type fringes [7]. Hence, further experiments are desirable. Quantum beats in the intensity are the result of the inability to tell the path of a particular photon when observed by a broadband detector. The beats can also occur in two-time correlations. As a general rule, initial conditions should be a superposition state.

In this paper we investigate theoretically effects of quantum interference on the total intensity and two-time correlations such as dipole-dipole (to calculate spectra), intensity-intensity, intensity-amplitude correlations, and variance of the light emitted into the π transitions of the $J = 1/2 - J' = 1/2$ atomic system driven by a linearly polarized laser and a magnetic field to break the degeneracy. While we put emphasis on the regime of observation of quantum beats, the nonclassical and non-Gaussian properties of the fluorescence are also investigated.

After describing the main features of the model in Section II, we discuss the basic dynamic and stationary properties of the atomic expectation values in Section III. Here, we analyze the previously overlooked time-dependent behavior of the atomic populations. Those of the excited states, for instance, although equal in the steady state, evolve with different Rabi frequencies and amplitudes. This is at the root of the formation of beats in the intensity and the correlations. In the regime of strong laser and magnetic fields these beats are characterized by well-defined oscillations at the *average* frequency among two generalized Rabi frequencies, modulated at the difference of those frequencies. To observe beats in the intensity both ground state populations must be nonzero initially, ideally equal [1]. Similarly, for the two-time correlations, the vector of initial conditions must

* hcastro@uaem.mx

have at least two nonzero terms.

In Section IV we describe the scattered field intensity and quadratures. Here, beats depend only on the interference of the two upper populations in the nondegenerate case, with both lower populations initially nonzero. Cross terms of the opposite π transitions represent interference in the steady state intensity. Then, In Section V, using the dressed states approach, we show that the double sideband spectrum [5] stems from a dipole-dipole correlation with beats, where the terms of addition of single π transitions dominate over those of the cross terms.

In Section VI we study Brown-Twiss photon-photon correlations [16, 17], extending the work of Ref.[8] to the nondegenerate case. Besides the ubiquitous antibunching effect, for weak to moderate laser drivings the interplay of parameters, together with detuning and Zeeman splittings, can make for somewhat involved evolutions, e.g., long decays due to optical pumping in the non-degenerate case. Again, cross terms are minor contributors to the full correlation in the beats regime.

Section VII is devoted to a study of phase-dependent fluctuations by conditional homodyne detection (CHD) [18, 19] in both the temporal and spectral domains. The CHD method is characterized by amplitude-intensity correlations (AIC), which are of third order in the field amplitude. When the atomic operators are decomposed into a mean plus a noise operator the AIC is split into a second-order term which would be a measure of squeezing if the third-order one were negligible. But the latter is not negligible outside the weak field regime of resonance fluorescence, which make the fluctuations non-Gaussian and also nonclassical by the violation of classical inequalities [20]. We obtain the spectra of the total, second- and third-order terms of the AIC. Narrow peaks in the spectra reveal population trapping when detunings favour the long term population or optical pumping of the ground state of the more detuned transition, which in the time domain show the above mentioned long decays. The third-order terms make up most of the beats and thus they are non-Gaussian and nonclassical but not squeezed.

In Section VIII we consider squeezing by means of the variance of fluctuations. As usual, squeezing in resonance fluorescence is small and restricted to weak or moderate Rabi frequencies. Finally, in Section IX we provide a discussion and conclusions, and two Appendices give details on solution methods, initial conditions, and optimal appearance of beats.

II. MODEL

The system, illustrated in Fig. 1, consists of a two-level atom with transition $J = 1/2 - J = 1/2$ and states with magnetic quantum number $m = \pm J$,

$$\begin{aligned} |1\rangle &= |J, -1/2\rangle, & |2\rangle &= |J, 1/2\rangle, \\ |3\rangle &= |J, -1/2\rangle, & |4\rangle &= |J, 1/2\rangle. \end{aligned} \quad (1)$$

The matrix elements are

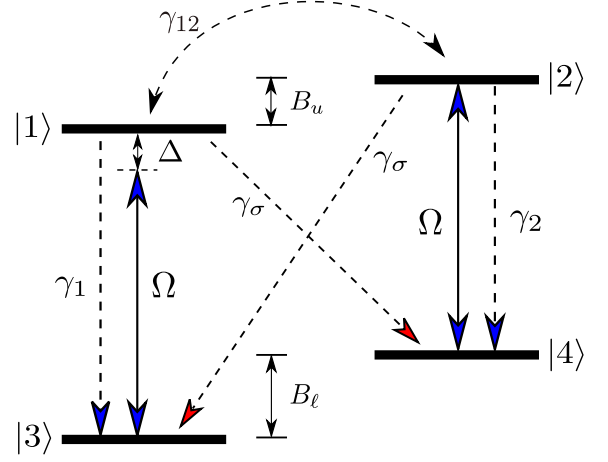


FIG. 1. Scheme of the $J = 1/2 - J = 1/2$ atomic system interacting with a laser driving the $|1\rangle - |3\rangle$ and $|2\rangle - |4\rangle$ transitions with Rabi frequency Ω and detuning Δ . There are spontaneous decay rates γ_1 , γ_2 and γ_σ , vacuum-induced coherence γ_{12} , and Zeeman frequency splittings B_ℓ and B_u .

$$\begin{aligned} \mathbf{d}_1 &= \langle 1|\hat{\mathbf{d}}|3\rangle = -\frac{1}{\sqrt{3}}\mathcal{D}\mathbf{e}_z, & \mathbf{d}_2 &= \langle 2|\hat{\mathbf{d}}|4\rangle = -\mathbf{d}_1, \\ \mathbf{d}_3 &= \langle 2|\hat{\mathbf{d}}|3\rangle = \sqrt{\frac{2}{3}}\mathcal{D}\mathbf{e}_-, & \mathbf{d}_4 &= \langle 1|\hat{\mathbf{d}}|4\rangle = \mathbf{d}_3^*, \end{aligned} \quad (2)$$

where \mathcal{D} is the reduced dipole matrix element. We choose the field polarization basis $\{\mathbf{e}_z, \mathbf{e}_-, \mathbf{e}_+\}$ (linear, left circular, right circular), where $\mathbf{e}_\pm = \mp(\mathbf{e}_x \pm i\mathbf{e}_y)/2$.

The π transitions, $|1\rangle - |3\rangle$ and $|2\rangle - |4\rangle$ ($m = m'$), are coupled to linearly polarized light and have their dipole moments antiparallel. On the other hand, the σ transitions, $|1\rangle - |4\rangle$ and $|2\rangle - |3\rangle$ ($m \neq m'$), are coupled to circularly polarized light. This configuration can be found, for example, in $^{198}\text{Hg}^+$ [3], and $^{40}\text{Ca}^+$ [12].

The level degeneracy is removed by the application of a static magnetic field B_z along the z direction, the Zeeman effect. Note that the energy splittings $g\mu_B B_z$ of the upper (u) and lower (ℓ) levels are different due to unequal Landé g factors, g_u and g_ℓ , respectively; μ_B is Bohr's magneton. The difference Zeeman splitting is

$$\delta = \frac{(g_u - g_\ell)\mu_B B_z}{\hbar} = \frac{g_u - g_\ell}{g_\ell} B_\ell, \quad (3)$$

where $B_\ell = g_\ell\mu_B B_z/\hbar$. For $^{198}\text{Hg}^+$ $g_u = 2/3$ and $g_\ell = 2$, so $\hbar\delta = -(4/3)\mu_B B_z = -(2/3)\hbar B_\ell$.

The atom is driven by a monochromatic laser of frequency ω_L , linearly polarized in the z direction, propagating in the x direction,

$$\mathbf{E}_L(x, t) = E_0 e^{i(\omega_L t - k_L x)} \mathbf{e}_z + \text{c.c.}, \quad (4)$$

thus driving only the π transitions.

The free atomic, H_0 , and interaction, V , parts of the Hamiltonian are, respectively:

$$H_0 = \hbar\omega_{13}A_{11} + \hbar(\omega_{24} + B_\ell)A_{22} + \hbar B_\ell A_{44}, \quad (5)$$

$$V = \hbar\Omega(A_{13} - A_{24})e^{i\omega_L t} + \text{h.c.} \quad (6)$$

where $A_{jk} = |j\rangle\langle k|$ are atomic operators, ω_{13} and $\omega_{24} = \omega_{13} + \delta$ are the frequencies of the $|1\rangle - |3\rangle$ and $|2\rangle - |4\rangle$ transitions, respectively, and $\Omega = E_0 \mathcal{D} / \sqrt{3} \hbar$ is the Rabi frequency. The frequencies of the other transitions are $\omega_{23} = \omega_{13} - \delta$ and $\omega_{14} = \omega_{13} - B_\ell$. Using the unitary transformation

$$U = \exp[(A_{11} + A_{22})i\omega_L t], \quad (7)$$

the Hamiltonian in the frame rotating at the laser frequency is

$$\begin{aligned} H &= U^\dagger(H_0 + V)U, \\ &= -\hbar\Delta A_{11} - \hbar(\Delta - \delta)A_{22} + \hbar B_\ell(A_{22} + A_{44}) \\ &\quad + \hbar\Omega[(A_{13} - A_{24}) + \text{h.c.}], \end{aligned} \quad (8)$$

where $\Delta = \omega_L - \omega_{13}$ is the detuning of the laser from the $|1\rangle - |3\rangle$ resonance transition, and $\Delta - \delta$ is the detuning on the $|2\rangle - |4\rangle$ transition.

The excited states decay either in the π transitions emitting photons with linear polarization at rates $\gamma_1 = \gamma_2$, or in the σ transitions emitting photons of circular polarization at rate γ_σ . There is also a cross-coupling of the excited states by the reservoir, responsible for the quantum interference we wish to study. In general, the decay rates are written as

$$\gamma_{ij} = \frac{\mathbf{d}_i \cdot \mathbf{d}_j^*}{|\mathbf{d}_i||\mathbf{d}_j|} \sqrt{\gamma_i \gamma_j}, \quad i, j = 1, 2. \quad (9)$$

In particular, we have $\gamma_{ii} = \gamma_1 = \gamma_2$ and $\gamma_{13} = \gamma_{24} = \gamma_\sigma$. Also, given that \mathbf{d}_1 and \mathbf{d}_2 are antiparallel, $\gamma_{12} = \gamma_{21} = -\sqrt{\gamma_1 \gamma_2} = -\gamma_1$.

The total decay rate is

$$\gamma = \gamma_1 + \gamma_\sigma = \gamma_2 + \gamma_\sigma. \quad (10)$$

The decays for the π and σ transitions occur with the branching fractions b_π and b_σ [5], respectively,

$$\gamma_1 = \gamma_2 = b_\pi \gamma, \quad b_\pi = 1/3, \quad (11a)$$

$$\gamma_\sigma = b_\sigma \gamma, \quad b_\sigma = 2/3. \quad (11b)$$

III. MASTER EQUATION

The dynamics of the atom-laser-reservoir system is described by the master equation for the reduced atomic density operator, ρ . In a frame rotating at the laser frequency ($\tilde{\rho} = U\rho U^\dagger$) it is given by

$$\dot{\tilde{\rho}} = -\frac{i}{\hbar}[H, \tilde{\rho}] + \mathcal{L}_\gamma \tilde{\rho}, \quad (12)$$

where $-(i/\hbar)[H, \tilde{\rho}]$ describes the coherent atom-laser interaction and $\mathcal{L}_\gamma \tilde{\rho}$ describes the damping due to spontaneous emission [5, 21]. Defining

$$\begin{aligned} S_1^- &= A_{31}, \quad S_2^- = A_{42}, \quad S_3^- = A_{32}, \quad S_4^- = A_{41}, \\ S_i^+ &= (S_i^-)^\dagger, \end{aligned} \quad (13)$$

the dissipative part is written as

$$\begin{aligned} \mathcal{L}_\gamma \tilde{\rho} &= \frac{1}{2} \sum_{i,j=1}^2 \gamma_{ij} (2S_i^- \tilde{\rho} S_j^+ - S_i^+ S_j^- \tilde{\rho} - \tilde{\rho} S_i^+ S_j^-) \\ &\quad + \frac{\gamma_\sigma}{2} \sum_{i=3}^4 (2S_i^- \tilde{\rho} S_i^+ - S_i^+ S_i^- \tilde{\rho} - \tilde{\rho} S_i^+ S_i^-). \end{aligned} \quad (14)$$

We now define the Bloch vector of the system as

$$\mathbf{Q} \equiv (A_{11}, A_{12}, A_{13}, A_{14}, A_{21}, A_{22}, A_{23}, A_{24}, A_{31}, A_{32}, A_{33}, A_{34}, A_{41}, A_{42}, A_{43}, A_{44})^T. \quad (15)$$

The equations for the expectation values of the atomic operators, $\langle A_{jk} \rangle = \tilde{\rho}_{kj}$, are the so-called Bloch equations, which we write as

$$\frac{d}{dt} \langle \mathbf{Q}(t) \rangle = \mathbf{M}_B \langle \mathbf{Q}(t) \rangle, \quad (16)$$

where \mathbf{M}_B is a matrix of coefficients of the full master equation, and the formal solution is

$$\langle \mathbf{Q}(t) \rangle = e^{\mathbf{M}_B t} \langle \mathbf{Q}(0) \rangle. \quad (17)$$

Since we are interested only in properties of the fluorescence emitted in the π transitions we use the simplifying fact, already noticed in [8], that these Bloch equations can be split into two decoupled homogeneous sets. Set 1 contains the equations for the populations and the coherences of the coherently driven π transitions; these are

$$\begin{aligned} \dot{\langle A_{11} \rangle} &= -\gamma \langle A_{11} \rangle + i\Omega(\langle A_{31} \rangle - \langle A_{13} \rangle), \\ \dot{\langle A_{13} \rangle} &= -\left(\frac{\gamma}{2} + i\Delta\right) \langle A_{13} \rangle - i\Omega(\langle A_{11} \rangle - \langle A_{33} \rangle), \\ \dot{\langle A_{22} \rangle} &= -\gamma \langle A_{22} \rangle - i\Omega(\langle A_{42} \rangle - \langle A_{24} \rangle), \\ \dot{\langle A_{24} \rangle} &= -\left(\frac{\gamma}{2} + i(\Delta - \delta)\right) \langle A_{24} \rangle + i\Omega(\langle A_{22} \rangle - \langle A_{44} \rangle), \\ \dot{\langle A_{31} \rangle} &= -\left(\frac{\gamma}{2} - i\Delta\right) \langle A_{31} \rangle + i\Omega(\langle A_{11} \rangle - \langle A_{33} \rangle), \\ \dot{\langle A_{33} \rangle} &= \gamma_1 \langle A_{11} \rangle + \gamma_\sigma \langle A_{22} \rangle - i\Omega(\langle A_{31} \rangle - \langle A_{13} \rangle), \\ \dot{\langle A_{42} \rangle} &= -\left(\frac{\gamma}{2} - i(\Delta - \delta)\right) \langle A_{42} \rangle - i\Omega(\langle A_{22} \rangle - \langle A_{44} \rangle), \\ \dot{\langle A_{44} \rangle} &= \gamma_\sigma \langle A_{11} \rangle + \gamma_2 \langle A_{22} \rangle + i\Omega(\langle A_{42} \rangle - \langle A_{24} \rangle). \end{aligned} \quad (18)$$

with Bloch vector

$$\mathbf{R} \equiv (A_{11}, A_{13}, A_{22}, A_{24}, A_{31}, A_{33}, A_{42}, A_{44})^T \quad (19)$$

and a corresponding matrix \mathbf{M} , Eq. (A3). Equations (18) do not depend on γ_{12} , the vacuum-induced coupling of the upper levels, but on the applied magnetic field only through the difference of Zeeman splittings, δ .

The steady state solutions, for which we introduce the

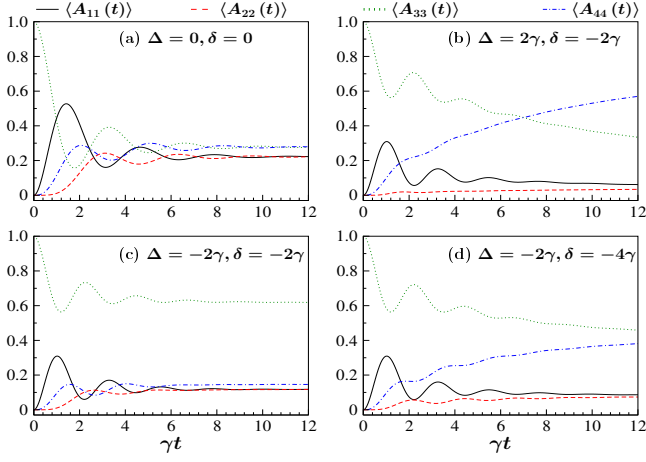


FIG. 2. Time-dependent populations $\langle A_{11}(t) \rangle$ (solid-black), $\langle A_{22}(t) \rangle$ (dashed-red), $\langle A_{33}(t) \rangle$ (dots-green), and $\langle A_{44}(t) \rangle$ (dashed-dots-blue), with the atom initially in state $|3\rangle$. The parameters are: $\Omega = \gamma$ and (a) $\Delta = \delta = 0$; (b) $\Delta = 2\gamma$, $\delta = -2\gamma$; (c) $\Delta = \delta = -2\gamma$; (d) $\Delta = -2\gamma$, $\delta = -4\gamma$.

short notation $\alpha_{jk} = \langle A_{jk} \rangle_{st}$, are

$$\alpha_{11} = \alpha_{22} = \frac{\Omega^2}{2D}, \quad (20a)$$

$$\alpha_{33} = \frac{\Omega^2 + \gamma^2/4 + \Delta^2}{2D}, \quad (20b)$$

$$\alpha_{44} = \frac{\Omega^2 + \gamma^2/4 + (\Delta - \delta)^2}{2D}, \quad (20c)$$

$$\alpha_{13} = \frac{\Omega(\Delta + i\gamma/2)}{2D}, \quad (20d)$$

$$\alpha_{24} = \frac{\Omega(\delta - \Delta - i\gamma/2)}{2D}, \quad (20e)$$

$$\alpha_{kj} = \alpha_{jk}^*.$$

where

$$D = 2\Omega^2 + \frac{\gamma^2 + \delta^2}{4} + \left(\Delta - \frac{\delta}{2}\right)^2. \quad (21)$$

Note also that in the degenerate system ($\delta = 0$) $\alpha_{33} = \alpha_{44}$ and that $\alpha_{31} = -\alpha_{42}$, where the minus sign arises from the fact that the dipole moments \mathbf{d}_1 and \mathbf{d}_2 are antiparallel.

Set 2 contains the equations for the coherences of the σ transitions and those among both upper and both lower levels,

$$\mathbf{R}_2 \equiv (A_{12}, A_{14}, A_{21}, A_{23}, A_{32}, A_{34}, A_{41}, A_{43})^T. \quad (22)$$

The equations for their expected values do depend on B_ℓ and γ_{12} . These coherences vanish because the σ transitions are driven incoherently ($\langle \{A_{14}, A_{23}, A_{32}, A_{41}\} \rangle$), i.e., by spontaneous emission, or because they are mediated by those σ transitions ($\langle \{A_{12}, A_{21}, A_{34}, A_{43}\} \rangle$). For completeness, we write the steady state results:

$$\alpha_{12} = \alpha_{34} = \alpha_{14} = \alpha_{23} = 0, \quad \alpha_{kj} = \alpha_{jk}^*. \quad (23)$$

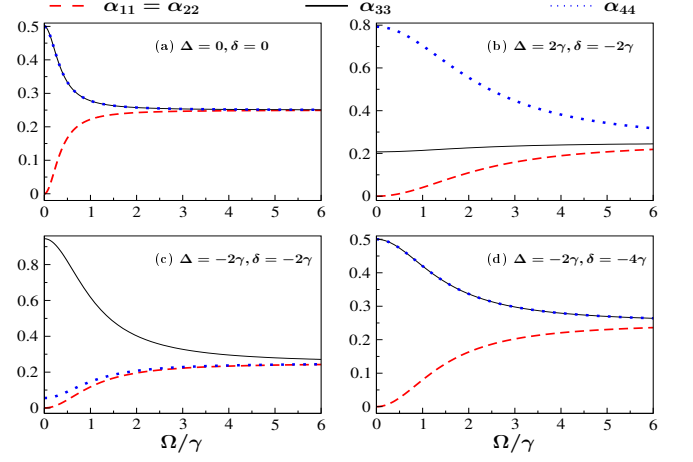


FIG. 3. Steady-state populations as a function of Rabi frequency: $\alpha_{11} = \alpha_{22}$ (dashed-red), α_{33} (solid-black), and α_{44} (dots-blue). All other parameters as in Fig. 2.

The properties of the fluorescence of the π transitions, the subject matter of this article, do not depend on the equations for Set 2. Only the second- and third-order amplitude-intensity correlations and the dipole correlation for the spectrum of the σ transitions would require the full set of Bloch equations.

We gain valuable information on the nontrivial dynamics of the atomic system from single-time expectation values, apparently ignored in the previous literature on the system. In Fig. 2 we show the populations for several particular cases, all with the atom initially in state $|3\rangle$. In the degenerate case, $\delta = 0$, the upper populations reach opposite phases by the end of the first Rabi cycle, Fig. 2(a). This is understandable since the electron occupation of, say, state $|1\rangle$ implies not to be in state $|2\rangle$, and viceversa. The same occurs for the lower populations. Next, we show three situations for the nondegenerate case with $\delta < 0$ (as it is for $^{198}\text{Hg}^+$). In Fig. 2(b) the laser is slightly detuned above the $|1\rangle - |3\rangle$ transition, but highly detuned from the $|2\rangle - |4\rangle$ transition; the oscillations get out of phase and most of the population ends up in state $|4\rangle$ by optical pumping. In Fig. 2(c) the laser is detuned below the $|1\rangle - |3\rangle$ transition, and the $|2\rangle - |4\rangle$ transition is now on resonance with the laser; again, the oscillations are out of phase but most of the population ends up now in state $|3\rangle$. In Fig. 2(d) we extend the previous case but with stronger applied magnetic field, thus the non-degeneracy is more evident; the large detuning on both transitions makes it recover the opposite phases of the degenerate case.

In Fig. 3 we show the steady state populations as a function of the Rabi frequency; the other parameters are the same as in Fig. 2. For strong fields the populations tend to be equal ($1/4$), but arrive at that limit at different rates; for instance, for large detunings on both transitions, Fig. 3(d), it takes larger fields, as compared to the degenerate case, Fig. 3(a). On the other hand, for small detunings and weak-moderate fields, when one

transition is closer to resonance than the other, the lower state of the more detuned transition is more populated, as seen in Figs. 3 (b) and (c).

IV. THE SCATTERED FIELD

In this Section we present the main dynamical and stationary properties of the field scattered by the atom, with emphasis on the π transitions.

A. Single-Time and Stationary Properties

The positive-frequency part of the emitted field operator is [5, 21]

$$\hat{E}^+(\mathbf{r}, t) = \hat{E}_{\text{free}}^+(\mathbf{r}, t) + \hat{E}_S^+(\mathbf{r}, \hat{t}), \quad (24)$$

where $\hat{E}_{\text{free}}^+(\mathbf{r}, t)$ is the free-field part, which does not contribute to normally ordered correlations, hence we omit it in further calculations, and

$$\hat{E}_S^+(\mathbf{r}, t) = -\frac{\eta}{r} \sum_{i=1}^4 \omega_i^2 \hat{\mathbf{r}} \times (\hat{\mathbf{r}} \times \mathbf{d}_i) S_i^-(\hat{t}) \quad (25)$$

is the dipole source field operator in the far-field zone, where $\hat{t} = t - r/c$ is the retarded time and $\eta = (4\pi\epsilon_0 c^2)^{-1}$. Since $\omega_i \gg \delta$, we may approximate the four transition as a single one ω_0 in Eq. (25), but cannot do so at the level of decay rates, Rabi frequencies, and splittings.

Making $\hat{\mathbf{r}} = \mathbf{e}_y$ the direction of observation and using Eq. (2) we have

$$\hat{E}_S^+(\mathbf{r}, \hat{t}) = \hat{E}_\pi^+(\mathbf{r}, \hat{t}) \mathbf{e}_z + \hat{E}_\sigma^+(\mathbf{r}, \hat{t}) \mathbf{e}_x, \quad (26)$$

i.e., the fields scattered from the π and σ transitions are polarized in the \mathbf{e}_z and \mathbf{e}_x directions, respectively, where

$$\hat{E}_\pi^+(\mathbf{r}, \hat{t}) = f_\pi(r) [A_{31}(\hat{t}) - A_{42}(\hat{t})], \quad (27a)$$

$$\hat{E}_\sigma^+(\mathbf{r}, \hat{t}) = f_\sigma(r) [A_{32}(\hat{t}) - A_{41}(\hat{t})], \quad (27b)$$

are the positive-frequency source field operators of the π and σ transitions, and

$$f_\pi(r) = -\eta\omega_1^2 \mathcal{D}/\sqrt{3}r, \quad f_\sigma(r) = \sqrt{2}f_\pi(r), \quad (28)$$

are their geometric factors.

The intensity in the π transitions is given by

$$\begin{aligned} I_\pi(\mathbf{r}, \hat{t}) &= \langle \hat{E}_\pi^-(\mathbf{r}, \hat{t}) \cdot \hat{E}_\pi^+(\mathbf{r}, \hat{t}) \rangle \\ &= f_\pi^2(r) \langle A_{13}(\hat{t}) A_{31}(\hat{t}) + A_{24}(\hat{t}) A_{42}(\hat{t}) \rangle \\ &= f_\pi^2(r) \langle A_{11}(\hat{t}) + A_{22}(\hat{t}) \rangle, \end{aligned} \quad (29a)$$

while in the steady state is

$$I_\pi^{st} = f_\pi^2(r) [\alpha_{11} + \alpha_{22}] = \frac{\Omega^2}{D}. \quad (29b)$$

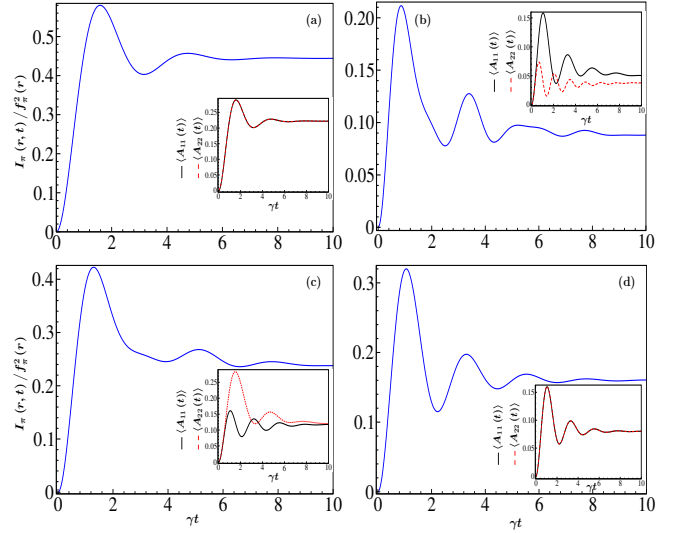


FIG. 4. Fluorescence intensity of the π transitions with equal initial ground state populations, $\langle A_{33}(0) \rangle = \langle A_{44}(0) \rangle = 1/2$. The other parameters are as in Fig. 2: $\Omega = \gamma$ and (a) $\Delta = \delta = 0$; (b) $\Delta = 2\gamma$, $\delta = -2\gamma$; (c) $\Delta = \delta = -2\gamma$; (d) $\Delta = -2\gamma$, $\delta = -4\gamma$. The insets show the excited states populations: $\langle A_{11}(t) \rangle$ (solid), $\langle A_{22}(t) \rangle$ (dashed).

Adding the excited state populations with the atom initially in the single state $|3\rangle$ in Eq. 29a gives simply $I_\pi(\mathbf{r}, \hat{t}) = f_\pi^2(r) \langle A_{11}(\hat{t}) \rangle$, i.e., without the contribution of $\langle A_{22}(\hat{t}) \rangle$. More interesting is the case where the initial condition is $\langle A_{33}(0) \rangle = \langle A_{44}(0) \rangle = 1/2$, shown in Fig. 4 (see the populations $\langle A_{11}(t) \rangle$ and $\langle A_{22}(t) \rangle$ in the insets). The modulation in the intensity is reminiscent of the quantum beats in the spontaneous decay in the V three-level system [1, 2]. These beats are basically due to the inability to tell from which of the π transitions a photon comes from. This is the standard Young-type interference [4, 5, 7]. The main requirement is that the initial condition for both ground states are nonzero (see Appendix B).

More interesting, though, is the case of strong resonant laser and magnetic fields and the laser is detuned far from the $|2\rangle - |4\rangle$ resonance frequency, shown in Fig. 5. Due to the laser detuning, the population $\langle A_{22}(t) \rangle$ has larger frequency and smaller amplitude than that of $\langle A_{11}(t) \rangle$, as seen in the insets. Remarkably well-defined wave-packets or beats are observed due to the interference of the fluorescence of both π transitions with close Rabi frequencies, with clear average and modulation frequencies (see Fig. 5a). The beats get scrambled with larger frequency and amplitude differences, Fig. 5b.

Save for the decay, these beats are more like the classic textbook ones, described by a modulation *and* an average frequency, unlike the beats from spontaneous emission or weak resonance fluorescence from two or more closely separated levels. Henceforth, we reserve the moniker *beats* to those due to strong applied fields. Further analyses of the beats are given in the next Sections, as they show up

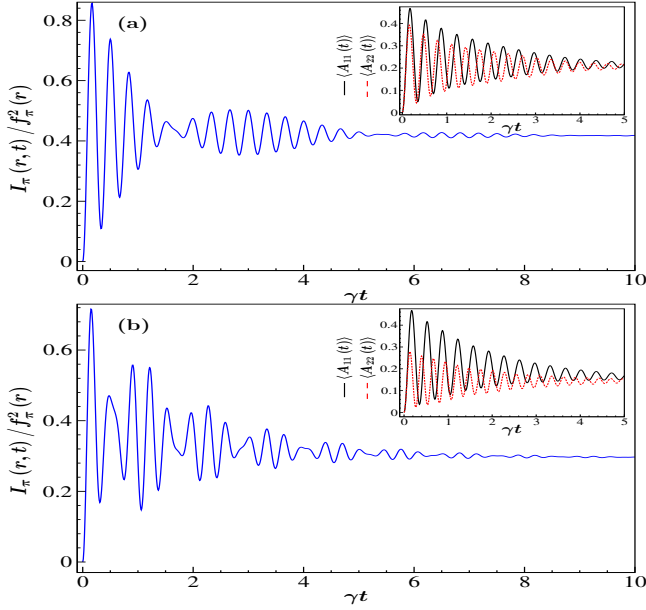


FIG. 5. Fluorescence intensity for $\Omega = 9\gamma$, $\Delta = 0$, and (a) $\delta = -8\gamma$ and (b) $\delta = -15\gamma$. The insets show the excited state populations $\langle A_{11} \rangle$ (solid line) and $\langle A_{22} \rangle$ (dotted line). The initial conditions are $\langle A_{33}(0) \rangle = \langle A_{44}(0) \rangle = 1/2$, $\langle A_{11}(0) \rangle = \langle A_{22}(0) \rangle = 0$.

also in two-time correlations with particular features.

Similarly, for the σ transitions we have

$$\begin{aligned} I_\sigma(\mathbf{r}, \hat{t}) &= \langle \hat{E}_\sigma^-(\mathbf{r}, \hat{t}) \cdot \hat{E}_\sigma^+(\mathbf{r}, \hat{t}) \rangle \\ &= f_\sigma^2(r) [\langle A_{23}(\hat{t}) A_{32}(\hat{t}) + A_{14}(\hat{t}) A_{41}(\hat{t}) \rangle] \\ &= f_\sigma^2(r) [\langle A_{11}(\hat{t}) + A_{22}(\hat{t}) \rangle], \end{aligned} \quad (30a)$$

$$I_\sigma^{st} = f_\sigma^2(r) [\alpha_{11} + \alpha_{22}], \quad (30b)$$

also showing beats with intensity twice that of the π transitions given that $f_\sigma^2(r) = 2f_\pi^2(r)$.

The field quadrature operator at any time is

$$\begin{aligned} \hat{E}_{\pi, \phi}(\mathbf{r}, \hat{t}) &= \frac{1}{2} (E_\pi^-(\mathbf{r}, \hat{t}) e^{-i\phi} + E_\pi^+(\mathbf{r}, \hat{t}) e^{i\phi}) \\ &= f_\pi(r) (S_{1, \phi} - S_{2, \phi}), \end{aligned} \quad (31)$$

where $\phi = 0, \pi/2$ are the quadrature phases we consider, and

$$S_{1, \phi} = \frac{1}{2} (A_{13} e^{-i\phi} + A_{31} e^{i\phi}), \quad (32a)$$

$$S_{2, \phi} = \frac{1}{2} (A_{24} e^{-i\phi} + A_{42} e^{i\phi}). \quad (32b)$$

The mean quadrature field is given by

$$\begin{aligned} \langle \hat{E}_{\pi, \phi} \rangle_{st} &= \frac{f_\pi(r)}{2} [(\alpha_{13} - \alpha_{24}) e^{-i\phi} + (\alpha_{31} - \alpha_{42}) e^{i\phi}] \\ &= f_\pi(r) \text{Re} [(\alpha_{13} - \alpha_{24}) e^{-i\phi}] \\ &= f_\pi(r) \text{Re} \left[\frac{\Omega(\Delta + (i\gamma - \delta)/2)}{D} e^{-i\phi} \right], \end{aligned} \quad (33)$$

B. Intensity and Quadrature Fluctuations

Here we introduce the intensity and quadratures of the field in terms of atomic fluctuation operators $\Delta A_{jk} = A_{jk} - \langle A_{jk} \rangle_{st}$, such that

$$\langle A_{kl} A_{mn} \rangle = \alpha_{kl} \alpha_{mn} + \langle \Delta A_{kl} \Delta A_{mn} \rangle. \quad (34)$$

Only the π transitions have nonvanishing coherence terms ($\alpha_{13}, \alpha_{24} \neq 0$). The fluorescence in the σ transitions is fully incoherent ($\alpha_{14} = \alpha_{23} = 0$), so its intensity is given by Eq. (30b). In the remainder of this section we deal only with the π transition. The quadrature operators are then written as

$$\hat{E}_{\pi, \phi}(\mathbf{r}, \hat{t}) = f_\pi(r) [\alpha_{\pi, \phi} + \Delta S_{\pi, \phi}(\hat{t})], \quad (35a)$$

where

$$\alpha_{\pi, \phi} = \frac{1}{2} (\alpha_{31} - \alpha_{42}) e^{i\phi} + \frac{1}{2} (\alpha_{13} - \alpha_{24}) e^{-i\phi}, \quad (35b)$$

$$= \text{Re} \left[\frac{\Omega(\Delta + (i\gamma - \delta)/2)}{D} e^{-i\phi} \right],$$

$$\Delta S_{\pi, \phi} = \frac{1}{2} (\Delta A_{31} - \Delta A_{42}) e^{i\phi} + \frac{1}{2} (\Delta A_{13} - \Delta A_{24}) e^{-i\phi}. \quad (35c)$$

From Eqs. (29b) and (34) we write the steady state intensity in terms of products of dipole and dipole fluctuation operator expectation values,

$$I_\pi^{st}(\mathbf{r}) = f_\pi^2(r) [I_{\pi, 0}^{coh} + I_{\pi, 0}^{inc} + I_{\pi, cross}^{coh} + I_{\pi, cross}^{inc}], \quad (36)$$

where

$$I_{\pi, 0}^{coh} = |\langle A_{13} \rangle_{st}|^2 + |\langle A_{24} \rangle_{st}|^2, \quad (37a)$$

$$I_{\pi, 0}^{inc} = \langle \Delta A_{13} \Delta A_{31} \rangle + \langle \Delta A_{24} \Delta A_{42} \rangle, \quad (37b)$$

$$\begin{aligned} I_{\pi, cross}^{coh} &= -\langle A_{13} \rangle_{st} \langle A_{42} \rangle_{st} - \langle A_{24} \rangle_{st} \langle A_{31} \rangle_{st} \\ &= -2\text{Re} (\langle A_{13} \rangle_{st} \langle A_{42} \rangle_{st}), \end{aligned} \quad (37c)$$

$$\begin{aligned} I_{\pi, cross}^{inc} &= -\langle \Delta A_{13} \Delta A_{42} \rangle - \langle \Delta A_{24} \Delta A_{31} \rangle \\ &= -2\text{Re} (\langle \Delta A_{13} \Delta A_{42} \rangle). \end{aligned} \quad (37d)$$

Superindices *coh* and *inc* stand, respectively, for the coherent (depending on mean dipoles) and incoherent (depending on noise terms) parts of the emission. Subindex 0 stands for terms with the addition of single transition products, giving the total intensity, while subindex *cross* stands for terms with products of the two π transitions, the steady state interference part of the intensity. In

terms of atomic expectation values these intensities are:

$$I_{\pi,0}^{coh} = |\alpha_{13}|^2 + |\alpha_{24}|^2 \quad (38a)$$

$$= \frac{\Omega^2}{4D^2} \left[\frac{\gamma^2}{2} + \Delta^2 + (\delta - \Delta)^2 \right],$$

$$I_{\pi,0}^{inc} = \alpha_{11} + \alpha_{22} - |\alpha_{13}|^2 - |\alpha_{24}|^2 \quad (38b)$$

$$= \frac{\Omega^2}{D^2} \left[2\Omega^2 - \frac{\gamma^2}{4} - \Delta^2 - \delta^2 \right],$$

$$I_{\pi,cross}^{coh} = -2\text{Re}(\alpha_{13}\alpha_{42}) \quad (38c)$$

$$= \frac{\Omega^2}{2D^2} \left[\frac{\gamma^2}{4} + \Delta(\Delta - \delta) \right],$$

$$I_{\pi,cross}^{inc} = 2\text{Re}(\alpha_{13}\alpha_{42}) = -I_{\pi,cross}^{coh}, \quad (38d)$$

The sum of these terms is, of course, the total intensity, Eq. (29a). As usual in resonance fluorescence, the coherent and incoherent intensities are similar only in the weak field regime, $\Omega \leq \gamma$. Here, in particular, the term $I_{\pi,0}^{inc}$ (no interference) becomes much larger than the others for strong driving.

C. Degree of Interference - Coherent Part

In Ref. [5], a measure of the effect of interference in the coherent part of the intensity was as

$$I_{\pi,0}^{coh} + I_{\pi,cross}^{coh} = I_{\pi,0}^{coh}(1 + C(\delta)),$$

$$C(\delta) = \frac{I_{\pi,cross}^{coh}}{I_{\pi,0}^{coh}} = \frac{\gamma^2/4 + \Delta(\Delta - \delta)}{\gamma^2/4 + \delta^2/4 + (\Delta - \delta/2)^2}, \quad (39)$$

independent of the Rabi frequency and shown in Fig. 6(a).

Some special cases are found analytically:

$$C(0) = 1, \quad \delta = 0, \quad (40a)$$

$$C(\delta_0) = 0, \quad \delta_0 = \Delta[1 + (\gamma/2\Delta)^2], \quad (40b)$$

$$C(\delta_{min}) = \frac{-1}{1 + \gamma^2/2\Delta^2}, \quad \delta_{min} = 2\Delta[1 + (\gamma/2\Delta)^2], \quad (40c)$$

$$C(\delta_{1/2}^\pm) = 1/2, \quad \delta_{1/2}^\pm = -\Delta \pm \sqrt{3\Delta^2 + (\gamma^2/2)}. \quad (40d)$$

In the degenerate case, $C(\delta = 0) = 1$ means perfect constructive interference. That is because at $\delta = 0$ both π transitions (and both σ transitions) share the same reservoir environment. Increasing δ the reservoir overlap decreases, so is the interference. Negative values of C indicate destructive interference; its minimum is given by δ_{min} . For large detunings, $\Delta^2 \gg \gamma^2$ we have

$$\delta_0 = \Delta, \quad \delta_{min} = 2\Delta, \quad \delta_{1/2}^\pm = -\Delta \pm \sqrt{3}|\Delta|. \quad (40e)$$

We have used the special cases $\delta = \{0, \delta_0, \delta_{min}\}$ as a guide to obtain many of the figures in this paper.

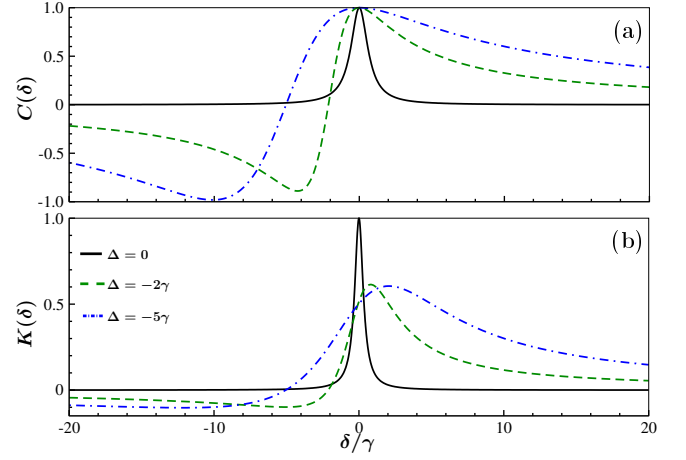


FIG. 6. Relative weight of the interference terms $C(\delta)$ (a) and $K(\delta)$ (b). In (b) $\Omega = \gamma/4$. For $^{198}\text{Hg}^+$, $\delta \leq 0$.

D. Degree of Interference - Incoherent Part

Likewise, we define a measure, $K(\delta)$, of the effect of interference in the intensity's incoherent part,

$$I_{\pi,0}^{inc} + I_{\pi,cross}^{inc} = I_{\pi,0}^{inc}(1 + K(\delta)),$$

$$K(\delta) = \frac{I_{\pi,cross}^{inc}}{I_{\pi,0}^{inc}} = \frac{\gamma^2/4 + \Delta(\Delta - \delta)}{2[\gamma^2/4 + \delta^2 + \Delta^2 - 2\Omega^2]}. \quad (41)$$

Unlike $C(\delta)$, $K(\delta)$ also depends on the Rabi frequency as Ω^{-2} , since fluctuations increase with laser intensity. Special cases are:

$$K(0) = \frac{\gamma^2/4 + \Delta^2}{2[\gamma^2/4 + \Delta^2 - 2\Omega^2]}, \quad \delta = 0, \quad (42a)$$

$$K(\delta) = 0, \quad \delta = \Delta + \frac{\gamma^2}{4\Delta} \quad \text{or} \quad \Omega \gg \gamma, \Delta, \delta. \quad (42b)$$

The behavior of $K(\delta)$ with Δ is more subtle. It is basically required that $\Delta \sim \Omega$ in order to preserve the shape seen in Fig. 6(b), in which case the minima for $C(\delta)$ and $K(\delta)$ are very similar. On-resonance, for example, Ω should be no larger than 0.35γ . Also, we can infer that the beats are little affected by the interference term unless $\Delta \gtrsim \Omega \gg \gamma$.

V. TWO-TIME DIPOLE CORRELATIONS AND POWER SPECTRUM

The resonance fluorescence spectrum of the $J = 1/2 \rightarrow J = 1/2$ atomic system was first considered in [3] and then very thoroughly in [4, 5]. Thus, here we only consider basic definitions and issues related to the observation of beats.

The stationary Wiener-Khintchine power spectrum is given by the Fourier transform of the field autocorrelation function

$$S_\pi(\omega) = \text{Re} \int_0^\infty d\tau e^{-i\omega\tau} \langle \hat{E}_\pi^-(0) \hat{E}_\pi^+(\tau) \rangle, \quad (43)$$

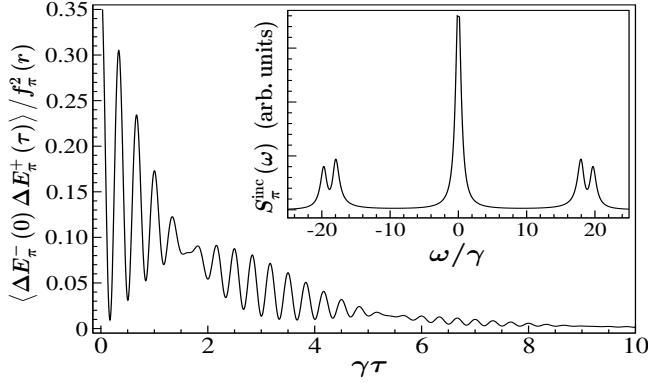


FIG. 7. Dipole correlation function $\langle \Delta \hat{E}_\pi^-(0) \Delta \hat{E}_\pi^+(\tau) \rangle$ for $\Omega = 9\gamma$, $\delta = -8\gamma$, and $\Delta = 0$. The inset shows the corresponding incoherent spectrum $S_\pi^{inc}(\omega)$.

such that $\int_{-\infty}^{\infty} S_\pi(\omega) d\omega = I_\pi^{st}$. By writing the atomic operators in Eq. (27a) as $A_{jk}(t) = \alpha_{jk} + \Delta A_{jk}(t)$, we separate the spectrum in two parts: a coherent one,

$$\begin{aligned} S_\pi^{coh}(\omega) &= \text{Re} \int_0^\infty e^{-i\omega\tau} d\tau [I_{\pi,0}^{coh} + I_{\pi,cross}^{coh}] \\ &= \pi [I_{\pi,0}^{coh} + I_{\pi,cross}^{coh}] \delta(\omega) \\ &= \frac{\pi\Omega^2}{D^2} \left[\frac{\gamma^2}{4} + \left(\Delta - \frac{\delta}{2} \right)^2 \right] \delta(\omega), \end{aligned} \quad (44)$$

due to elastic scattering, where $I_{\pi,0}^{coh}$ and $I_{\pi,cross}^{coh}$ are given by Eqs. (38) (a) and (c), respectively; and an incoherent part,

$$S_\pi^{inc}(\omega) = \text{Re} \int_0^\infty d\tau e^{-i\omega\tau} \langle \Delta \hat{E}_\pi^-(0) \Delta \hat{E}_\pi^+(\tau) \rangle,$$

specifically,

$$\begin{aligned} S_\pi^{inc}(\omega) &= \text{Re} \int_0^\infty d\tau e^{-i\omega\tau} [\langle \Delta A_{13}(0) \Delta A_{31}(\tau) \rangle \\ &\quad + \langle \Delta A_{24}(0) \Delta A_{42}(\tau) \rangle - \langle \Delta A_{13}(0) \Delta A_{42}(\tau) \rangle \\ &\quad - \langle \Delta A_{24}(0) \Delta A_{31}(\tau) \rangle], \end{aligned} \quad (45)$$

due to atomic fluctuations. An outline of the numerical calculation is given in Appendix A.

The dipole correlation $\langle \hat{E}_\pi^-(0) \hat{E}_\pi^+(\tau) \rangle$ and the incoherent spectrum in the strong driving regime and strong nondegeneracy (large δ) are shown in Fig. 7. The spectrum (inset) displays a central peak and two pairs of Mollow-like-sidebands [22] with peaks at the Rabi sidebands $\pm\Omega_1$ and $\pm\Omega_2$, while the correlation features decaying quantum beats due to the closeness of the Rabi peaks.

As usual in the strong-field regime, the dressed system approach allows to discern the origin of the peaks from the transitions among the dressed states, to find their positions [5], and thus find the frequencies of the beats. The generalized Rabi frequencies are

$$\Omega_1 = \mathcal{E}_1^+ - \mathcal{E}_1^- = \sqrt{4\Omega^2 + \Delta^2}, \quad (46a)$$

$$\Omega_2 = \mathcal{E}_2^+ - \mathcal{E}_2^- = \sqrt{4\Omega^2 + (\delta - \Delta)^2}, \quad (46b)$$

TABLE I. Eigenvalues of matrix \mathbf{M}/γ and initial conditions of the correlations in Eq. (45) for $\Omega = 9\gamma$ and $\Delta = 0$.

Eigenvalues	$\delta = -8\gamma$	$\delta = -15\gamma$
λ_1	$-0.749386 + 0i$	$-0.836531 + 0i$
λ_2	$-0.583099 - 18.0094i$	$-0.583308 - 17.9981i$
λ_3	$-0.583099 + 18.0094i$	$-0.583308 + 17.9981i$
λ_4	$-0.569785 - 19.6808i$	$-0.5492 - 23.4257i$
λ_5	$-0.569785 + 19.6808i$	$-0.5492 + 23.4257i$
λ_6	$-0.5 + 0i$	$-0.5 + 0i$
λ_7	$-0.444846 + 0i$	$-0.398452 + 0i$
λ_8	$0 + 0i$	$0 + 0i$
Init. cond.		
$\langle \Delta A_{13} \Delta A_{31} \rangle$	$0.20836 + 0i$	$0.14734 + 0i$
$\langle \Delta A_{24} \Delta A_{42} \rangle$	$0.174014 + 0i$	$0.086982 + 0i$
$\langle \Delta A_{13} \Delta A_{42} \rangle$	$0.000134 + 0.002146i$	$0.000067 + 0.002011i$
$\langle \Delta A_{24} \Delta A_{31} \rangle$	$0.000134 - 0.002146i$	$0.000067 - 0.002011i$

where

$$\mathcal{E}_1^\pm = -\frac{\Delta}{2} \pm \frac{1}{2} \sqrt{4\Omega^2 + \Delta^2}, \quad (47a)$$

$$\mathcal{E}_2^\pm = B_\ell + \frac{\delta - \Delta}{2} \pm \frac{1}{2} \sqrt{4\Omega^2 + (\delta - \Delta)^2}, \quad (47b)$$

are the eigenvalues of the Hamiltonian (8). Due to the spontaneous decays these frequencies would have to be corrected, but they are very good in the relevant strong field limit. Indeed, we notice that Ω_1 and Ω_2 are very close to the imaginary parts of the eigenvalues $\lambda_{2,3}$ and $\lambda_{4,5}$, respectively, of matrix \mathbf{M} , shown in Table I.

The beats are the result of the superposition of waves at the frequencies Ω_1 and Ω_2 of the spectral sidebands, with average frequency

$$\Omega_{av} = \frac{\Omega_2 + \Omega_1}{2} = \frac{\sqrt{4\Omega^2 + (\delta - \Delta)^2} + \sqrt{4\Omega^2 + \Delta^2}}{2}, \quad (48)$$

and beat or modulation frequency

$$\Omega_{beat} = \frac{\Omega_2 - \Omega_1}{2} = \frac{\sqrt{4\Omega^2 + (\delta - \Delta)^2} - \sqrt{4\Omega^2 + \Delta^2}}{2}. \quad (49)$$

Now, we can identify the origin and modulation frequency of the beats in the time-dependent intensity, Eq. (29a), since the excited state populations $\langle A_{11}(t) \rangle$ and $\langle A_{22}(t) \rangle$ oscillate at the generalized Rabi frequencies Ω_1 and Ω_2 , respectively, with initial conditions given by a nonzero superposition of ground state populations at $t = 0$. In the case of the dipole correlation $\langle \hat{E}_\pi^-(0) \hat{E}_\pi^+(\tau) \rangle$, however, the initial conditions are given by products of stationary atomic expectation values, most of them the coherences α_{13}, α_{24} , which become very small in the regime of beats. Thus, as seen in Table I, the terms $\langle \Delta A_{13}(0) \Delta A_{31}(\tau) \rangle$ and $\langle \Delta A_{24}(0) \Delta A_{42}(\tau) \rangle$ are

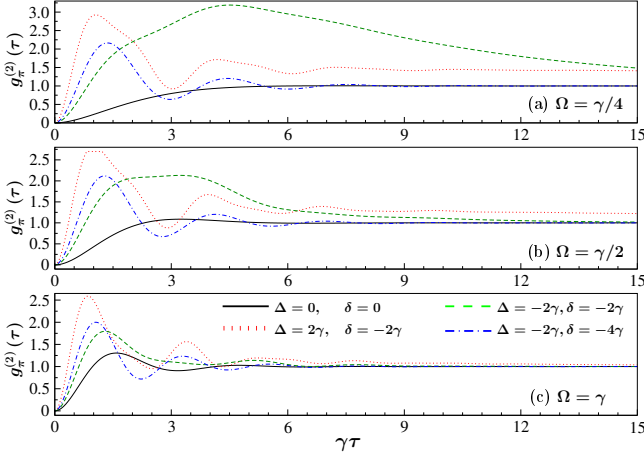


FIG. 8. Photon correlations for (a) $\Omega = 0.25\gamma$, (b) $\Omega = 0.5\gamma$ and (c) $\Omega = \gamma$. The pairs of values (Δ, δ) are the same as those in Fig. 2.

much larger than the cross terms $\langle \Delta A_{13}(0) \Delta A_{42}(\tau) \rangle$ and $\langle \Delta A_{24}(0) \Delta A_{31}(\tau) \rangle$, so the beats are basically due to the interference of those dominant terms.

VI. PHOTON-PHOTON CORRELATIONS

The standard method to investigate intensity fluctuations of a light source uses Brown-Twiss photon-photon correlations [16, 17]. The conditional character of this type of measurement makes it nearly free of detector inefficiencies, unlike a single-detector measurement of the photoelectron probability distribution. In Ref. [8] the correlations of two photons from the π transitions were studied, albeit only for the degenerate case. In this paper we extend it to the case of nondegenerate states. These correlations are defined as

$$g_{\pi}^{(2)}(\tau) = \frac{G_{\pi}^{(2)}(\tau)}{G_{\pi}^{(2)}(\tau \rightarrow \infty)} \quad (50)$$

where, using Eq. (27a) for the field operators,

$$\begin{aligned} G_{\pi}^{(2)}(\tau) &= \langle \hat{E}_{\pi}^{-}(0) \hat{E}_{\pi}^{-}(\tau) \hat{E}_{\pi}^{+}(\tau) \hat{E}_{\pi}^{+}(0) \rangle \\ &= f_{\pi}^4(r) \langle [A_{13}(0) - A_{24}(0)][A_{11}(\tau) + A_{22}(\tau)] \\ &\quad \times [A_{31}(0) - A_{42}(0)] \rangle, \end{aligned} \quad (51a)$$

and

$$G_{\pi}^{(2)}(\tau \rightarrow \infty) = (I_{\pi}^{st})^2 = f_{\pi}^4(r) (\alpha_{11} + \alpha_{22})^2 \quad (51b)$$

is the normalization factor. $G_{\pi}^{(2)}(\tau)$ can be further reduced, since $\langle A_{13} A_{jk}(\tau) A_{42}(0) \rangle = \langle A_{24} A_{jk}(\tau) A_{31}(0) \rangle = 0$, due to having vanishing initial conditions.

Figure 8 shows $g_{\pi}^{(2)}(\tau)$ for moderate values of the Rabi frequency (near saturation) and the same sets of detunings Δ and δ of Fig. 2. As usual in resonance fluorescence, the correlation shows antibunching, $g_{\pi}^{(2)}(0) = 0$,

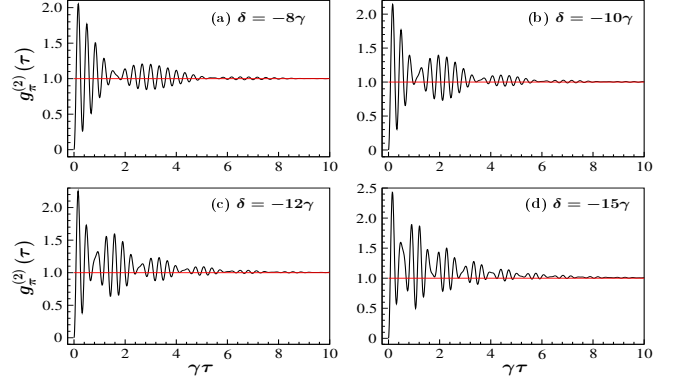


FIG. 9. Photon-photon correlations showing beats in the strong field limit, $\Omega = 9\gamma$, $\Delta = 0$, and large Zeeman splittings. The horizontal line helps to see that the wave packet is slightly risen.

that is, a single atom cannot emit two photons simultaneously. Unlike the two-level atom resonance fluorescence, the correlation is not simply the normalized population of the excited state, nor it is only the sum of the correlations of each single π transition. Besides the terms $\langle A_{13}(0) A_{11}(\tau) A_{31}(0) \rangle$ and $\langle A_{24}(0) A_{22}(\tau) A_{42}(0) \rangle$, which are also out of phase, as seen from the time-dependent populations of their excited states (Fig. 2), there are six cross terms in the full correlation. In the nondegenerate case the multiple contributions cause in some cases quite irregular evolution. For instance, as we will see in the next Section, the slow decay of the correlation when the laser drives the atom near saturation, but below the ω_{13} resonance transition, is related to a very narrow peak in the spectrum.

The case of strong driving and large nondegeneracy is shown in Fig. 9, featuring quantum beats. There are several effects resulting from the increase of the nondegeneracy factor δ : (i) the larger number of visible wave packets; (ii) both average and beat frequencies approach one another, so the wave packets get shorter for larger photon-pair intervals τ , containing very few of the fast oscillations, as seen in Fig. 9(d); (iii) the wavepackets are initially slightly lifted above the $g_{\pi}^{(2)}(\tau) = 1$ value.

VII. QUADRATURE FLUCTUATIONS

Squeezing, the reduction of noise in one quadrature below that of a coherent state at the expense of the other, is the hallmark of phase-dependent fluctuations of the electromagnetic field [cite]. It is usually measured by balanced homodyne detection (BHD), but low quantum detector efficiency degrade the weak squeezing produced in resonance fluorescence and cavity QED systems. One alternative our group has used is conditional homodyne detection (CHD) [18, 19], which correlates a quadrature amplitude on the cue of an intensity measurement. CHD measures a third-order amplitude-intensity corre-

lation (AIC) which, in the weak driving limit is reduced to the second-order one and that allows for measuring squeezing. Being a conditional measurement it is nearly free of detector inefficiencies.

While the original goal of CHD was to measure the weak squeezing in cavity QED [18, 19], it was soon realized that nonzero third-order fluctuations of the amplitude provide clear evidence of non-Gaussian fluctuations and higher-order field nonclassicality. In the present work the fluctuations are mainly third-order ones, due to near and above saturation excitation, and violate classical bounds. We thus explore the phase-dependent fluctuations under conditions of quantum interference following our recent work [20, 23, 24].

A. Amplitude-Intensity Correlations

In CHD a quadrature's field E_ϕ is measured by BHD on the cue of photon countings in a separate detector, where $\phi = 0, \pi/2$ is the phase of the local oscillator. This is characterized by a correlation among the amplitude and the intensity of the field,

$$h_{\pi,\phi}(\tau) = \frac{H_{\pi,\phi}(\tau)}{H_{\pi,\phi}(\tau \rightarrow \infty)}, \quad (52)$$

where

$$H_{\pi,\phi}(\tau) = \langle : \hat{E}_\pi^-(0) \hat{E}_\pi^+(0) \hat{E}_{\pi,\phi}(\tau) : \rangle, \quad (53a)$$

the dots $::$ indicating time and normal operator orderings, and

$$\begin{aligned} H_{\pi,\phi}(\tau \rightarrow \infty) &= I_\pi^{st} \langle E_{\pi,\phi} \rangle_{st} \\ &= f_\pi^3(r) [\alpha_{11} + \alpha_{22}] \text{Re} [(\alpha_{13} - \alpha_{24}) e^{-i\phi}] \\ &= f_\pi^3(r) \frac{\Omega^3}{D^2} \text{Re} [(\Delta + (i\gamma - \delta)/2) e^{-i\phi}] \end{aligned} \quad (53b)$$

is the normalization factor.

For the sake of concreteness, in this Section we limit our discussion to the out-of-phase quadrature, $\phi = \pi/2$, which is the one that features squeezing when $\omega_L = \omega_{13}$, that is $\Delta = 0$. We do consider, however, squeezing in the in-phase quadrature $\phi = 0$ in Sect. VIII on the variance.

In several atom-laser systems $h_{\pi,\phi}(\tau)$ has been proven to be time-asymmetric [20, 24]. This is not the case with the $J = 1/2 \rightarrow J = 1/2$ system so we limit the analysis to positive intervals $\tau \geq 0$. Omitting the geometrical factor $f_\pi^3(r)$, which is later cancelled by normalization, we have

$$\begin{aligned} H_{\pi,\phi}(\tau) &= \langle \hat{E}_\pi^-(0) \hat{E}_{\pi,\phi}(\tau) \hat{E}_\pi^+(0) \rangle \\ &= \text{Re} \{ e^{-i\phi} \langle A_{13}(0) [A_{13}(\tau) - A_{24}(\tau)] A_{31}(0) \\ &\quad + A_{24}(0) [A_{13}(\tau) - A_{24}(\tau)] A_{42}(0) \rangle \}. \end{aligned} \quad (54)$$

Note that $H_{\pi,\phi}(0) = 0$ meaning that, like antibunching in $g^{(2)}$, the atom has to build a new photon wavepacket after one has been emitted.

The AIC suggests nontrivial behavior when we take dipole fluctuations into account, that is, when the atomic operators are split into their mean plus noise, $A_{jk} = \alpha_{jk} + \Delta A_{jk}$; upon substitution in Eq. (54) we get

$$H_{\pi,\phi}(\tau) = I_\pi^{st} \langle E_{\pi,\phi} \rangle_{st} + H_{\pi,\phi}^{(2)}(\tau) + H_{\pi,\phi}^{(3)}(\tau), \quad (55)$$

or in normalized form as

$$h_{\pi,\phi}(\tau) = 1 + \frac{H_{\pi,\phi}^{(2)}(\tau)}{I_\pi^{st} \langle E_{\pi,\phi} \rangle_{st}} + \frac{H_{\pi,\phi}^{(3)}(\tau)}{I_\pi^{st} \langle E_{\pi,\phi} \rangle_{st}}, \quad (56)$$

where

$$\begin{aligned} H_{\pi,\phi}^{(2)}(\tau) &= 2\text{Re} \left[\langle \hat{E}_\pi^+ \rangle_{st} \langle \Delta \hat{E}_\pi^-(0) \Delta \hat{E}_{\pi,\phi}(\tau) \rangle \right] \\ &= \text{Re} \{ (\alpha_{31} - \alpha_{42}) [(\langle \Delta A_{13}(0) - \Delta A_{24}(0) \rangle (\Delta A_{13}(\tau) - \Delta A_{24}(\tau))) e^{-i\phi} \\ &\quad + \langle (\Delta A_{13}(0) - \Delta A_{24}(0)) (\Delta A_{31}(\tau) - \Delta A_{42}(\tau)) \rangle e^{i\phi}] \}, \end{aligned} \quad (57)$$

$$\begin{aligned} H_{\pi,\phi}^{(3)}(\tau) &= \langle \Delta \hat{E}_\pi^-(0) \Delta \hat{E}_{\pi,\phi}(\tau) \Delta \hat{E}_\pi^+(0) \rangle \\ &= \text{Re} \{ e^{i\phi} \langle [\Delta A_{13}(0) - \Delta A_{24}(0)] [\Delta A_{31}(\tau) - \Delta A_{42}(\tau)] [\Delta A_{31}(0) - \Delta A_{42}(0)] \rangle \}. \end{aligned} \quad (58)$$

The initial conditions of the correlations are given in Appendix A.

From $h_{\pi,\pi/2}(0) = 0$ we can obtain analytically the ini-

tial values of the second- and third-order terms,

$$h_{\pi,\pi/2}^{(2)}(0) = 1 - \frac{(2\Delta - \delta)^2 + \gamma^2}{2D}, \quad (59)$$

$$h_{\pi,\pi/2}^{(3)}(0) = \frac{(2\Delta - \delta)^2 + \gamma^2}{2D} - 2, \quad (60)$$

where D is given by Eq. (21).

Being the AIC a function of odd-order in the field amplitude we rightly expect a richer landscape than that of the intensity correlations, more so when one considers quantum interference and the complex parameter space. For instance, the correlation can take on not only negative values but break classical bounds [18, 19]:

$$0 \leq h_\phi(\tau) - 1 \leq 1, \quad (61a)$$

$$|h_\phi^{(2)}(\tau) - 1| \leq |h_\phi^{(2)}(0) - 1| \leq 1, \quad (61b)$$

where the second line is valid only for weak fields such that $h_\phi^{(3)}(\tau) \sim 0$. These classical bounds are stronger criteria for nonclassicality of the emitted field than squeezed light measurements, the more familiar probing of phase-dependent fluctuations. A detailed hierarchy of nonclassicality measures for higher-order correlation functions is presented in Refs. [25, 26]. In Ref. [20] an inequality was obtained that considers the full $h_\phi(\tau)$ by calculating the AIC for a field in a coherent state,

$$-1 \leq h_\phi(\tau) \leq 1. \quad (62)$$

For a meaningful violation of Poisson statistics, $h_\phi(\tau)$ must be outside these bounds.

Also, $h_\phi(\tau)$ is a measure of non-Gaussian fluctuations, here of third-order in the field fluctuations. Resonance fluorescence is a particularly strong case of non-Gaussian noise by being a highly nonlinear stationary nonequilibrium process [20, 23, 24, 27, 28], thanks also to its small Hilbert space. This makes resonance fluorescence unsuitable to a quasiprobability distribution approach.

B. Fluctuations Spectra

Since quadrature fluctuations, such as squeezing, are often studied in the frequency domain we now define the spectrum of the amplitude-intensity correlations:

$$S_{\pi,\phi}(\omega) = 8\gamma_1 \int_0^\infty d\tau \cos(\omega\tau) [h_{\pi,\phi}(\tau) - 1] \quad (63)$$

which, following Eqs. (52) and (55), can be decomposed into terms of second- and third-order in the dipole fluctuations

$$S_{\pi,\phi}^{(q)}(\omega) = 8\gamma_1 \int_0^\infty d\tau \cos(\omega\tau) h_{\pi,\phi}^{(q)}(\tau), \quad (64)$$

where $q = 2, 3$, so that $S_{\pi,\phi}(\omega) = S_{\pi,\phi}^{(2)}(\omega) + S_{\pi,\phi}^{(3)}(\omega)$.

As mentioned above, the AIC was devised initially to measure squeezing without the issue of imperfect detection efficiencies. Obviously, $h_{\pi,\phi}(\tau)$ and $S_{\pi,\phi}(\omega)$ are not measures of squeezing. They measure a third-order moment in the field's amplitude, while squeezing is a second-order one in its fluctuations. The so-called spectrum of squeezing is the one for $q = 2$, with the advantage of the AIC of not depending on the efficiency of detection. Squeezing is signaled by frequency intervals where

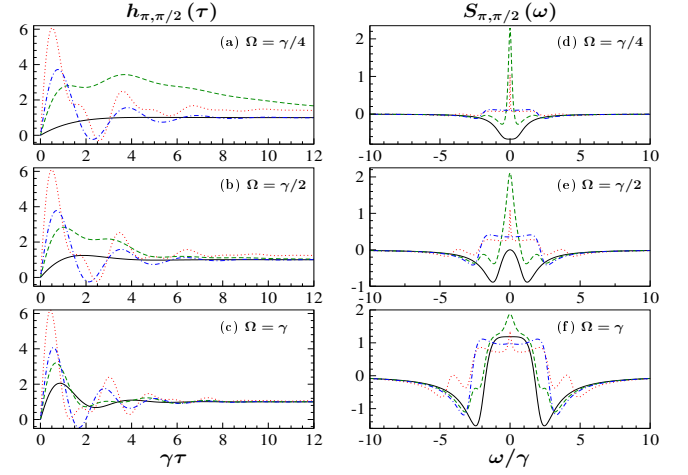


FIG. 10. Amplitude-intensity correlations (left panel) and spectra (right panel) for the $\phi = \pi/2$ quadrature in the weak-moderate field limit. Parameters and line styles are the same as in Fig. 8: $\Delta = \delta = 0$ (solid-black); $\Delta = 2\gamma$ and $\delta = -2\gamma$ (dots-red); $\Delta = -2\gamma$ and $\delta = -2\gamma$ (dashed-green); $\Delta = -2\gamma$ and $\delta = -4\gamma$ (dot-dashed-blue).

$S_{\pi,\phi}^{(2)}(\omega) < 0$. As a further note, the full incoherent spectrum, Eq. (45), can be obtained by adding the squeezing spectra of both quadratures [29],

$$S_{\pi}^{inc}(\omega) = \frac{1}{8\gamma_1} \left[S_{\pi,0}^{(2)}(\omega) + S_{\pi,\pi/2}^{(2)}(\omega) \right]. \quad (65)$$

C. Results

We now show plots of the AICs and their spectra in Figs. 10-12 for the $\phi = \pi/2$ quadrature and the same sets of detunings Δ, δ of Fig. 2, and weak to moderate Rabi frequencies, $\gamma/4 < \Omega < \gamma$. With the three parameters Ω, Δ , and δ , the landscape of effects is vast.

We first notice a few general features seen in $h_{\pi,\pi/2}(\tau)$, Fig. 10. With increasing Rabi frequencies, detunings, and Zeeman splittings we observe the clear breakdown of the classical inequalities besides the one at $\tau = 0$. Correspondingly, in the spectra, the extrema get displaced and broadened. Now, we want to single out the case of nondegeneracy with small detuning on the $|1\rangle - |3\rangle$ transition but large on the $|2\rangle - |4\rangle$ one, $\Delta = -\delta = 2\gamma$ (green-dashed line). For weak field, $\Omega = \gamma/4$, the AIC does not have a regular evolution for short times but it does decay very slowly, with a corresponding very narrow spectral peak. The slow decay is also clearly visible in the photon correlation, Fig. 8a. As we mentioned in Sect. III regarding Fig. 2b, state $|4\rangle$ ends up with a large portion of the steady state population due to optical pumping; not quite a trapping state, so there is no electron shelving *per se*, as argued in [5]. This effect is washed out for larger Rabi frequencies, which allow for faster recycling of the populations. To a lesser degree, slow decay and sharp peak occur for opposite signs of Δ and δ .

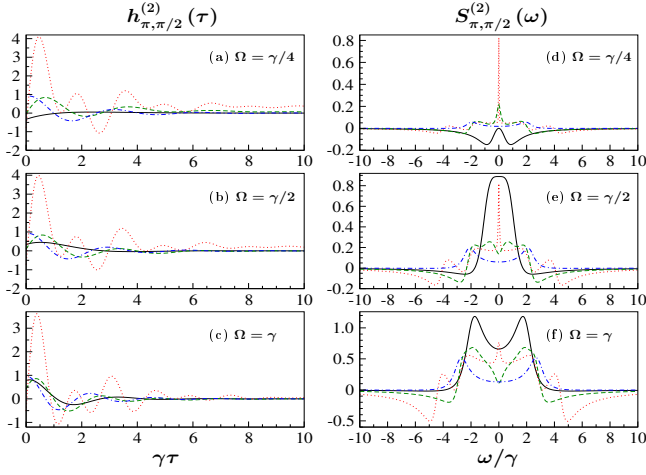


FIG. 11. Second-order component of the AIC and spectra of Fig. 10.

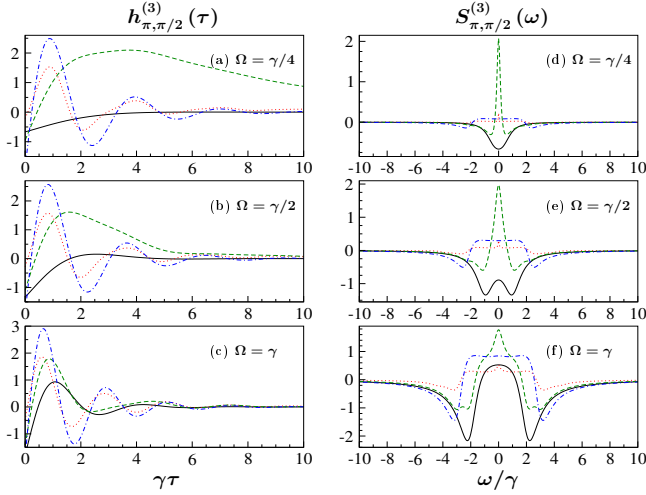


FIG. 12. Third-order component of the AIC and spectra of Fig. 10.

The splitting of the AIC and spectra into components of second and third order in the fluctuations, Figs. 11, 12, helps to understand better the quadrature fluctuations. For the second-order ones we have the squeezing spectra: around $\omega = 0$ for $\Delta = 0$ and small Rabi frequencies, $\Omega < \gamma/4$; and in sidebands for larger detunings, Rabi frequencies and Zeeman splittings. In $h_{\pi, \pi/2}^{(2)}(\tau)$ there is a reduction in amplitudes and nonclassicality for increasing Rabi frequencies except for the case of opposite signs of detuning and difference Zeeman splitting. Note that the sharp spectral peak in the latter case takes up most of the corresponding peak in Fig. 10. This is because both π transitions are largely detuned from the laser, keeping Ω small.

Increasing the laser strength the third-order effects overcome the second-order ones. For instance, regarding the size of the features. Also, a comparison of Figs. 11

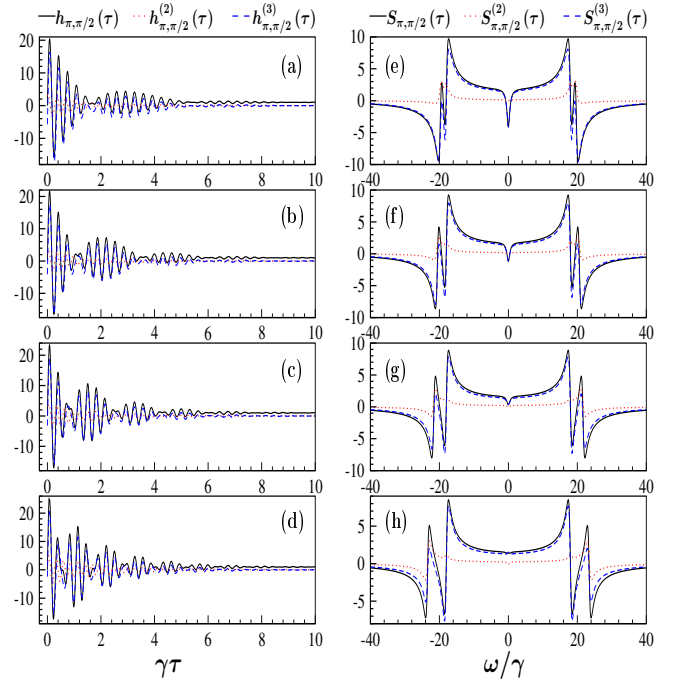


FIG. 13. AIC and spectra for $\Omega = 9\gamma$, $\Delta = 0$, (a,e) $\delta = -8\gamma$, (b,f) $\delta = -10\gamma$, (c,g) $\delta = -12\gamma$, (d,h) $\delta = -15\gamma$. Lines are: full AIC and spectra (solid-black), second-order (dots-red), and third-order (dashed-blue).

and 12 shows that $h_{\phi}^{(3)}(\tau)$ is mainly responsible for the breakdown of the classical bounds when the driving field is on or above saturation. Moreover, we see that the slow-decay-sharp-peak is mainly a third-order effect.

To close this Section, the AIC and spectra for very strong fields and large Zeeman splittings, $\Omega, |\delta| \gg \gamma$ are shown in Fig. 13. The AIC shows beats as in the photon correlations. Unlike those in $g^{(2)}(\tau)$, these wavepackets oscillate around $h(\tau) = 1$. Because the regime is that of strong excitation the third-order component clearly dominates, making the fluorescence notably non-Gaussian, and clearly violates the classical inequalities. The spectral peaks are localized around the Rabi frequencies $\pm\Omega_1, \pm\Omega_2$. Studies of the spectrum of squeezing for the $J = 1/2 - J = 1/2$ system were reported in [10]. Those authors choose $\pm\Omega_1, \pm\Omega_2$ with a less strong laser but large detuning and large Zeeman splittings, observing the double sidebands, but no mention or hint of beats was made.

VIII. VARIANCE

The variance is a measure of the total noise in a quadrature; it is defined as

$$V_{\phi} = \langle : (\Delta E_{\phi})^2 : \rangle = \text{Re} \left[e^{-i\phi} \langle \Delta \hat{E}^{-} \Delta \hat{E}_{\phi} \rangle_{st} \right], \quad (66)$$

and is related to the spectrum of squeezing as

$$V_\phi = \frac{1}{4\pi\gamma\eta} \int_{-\infty}^{\infty} d\omega S_\phi^{(2)}(\omega). \quad (67)$$

where η is the detector efficiency. The maximum value of V_ϕ is $1/4$, obtained when there is very strong driving, when almost all the emitted light is incoherent. Negative values of the variance are a signature of squeezing but, unlike the quadrature spectra, the squeezing is the total one in the field, independent of frequency.

For the π transitions we have

$$V_{\pi,\phi} = \frac{f_\pi^2(r)}{2} \text{Re} [-(\alpha_{13} - \alpha_{24})^2 e^{-2i\phi} + (\alpha_{11} + \alpha_{22} - |\alpha_{13} - \alpha_{24}|^2)], \quad (68)$$

$$= \frac{f_\pi^2(r)}{2} \frac{\Omega^2}{D} \left[1 - \frac{[(2\Delta - \delta) \cos \phi + \gamma \sin \phi]^2}{2D} \right]. \quad (69)$$

For $\phi = \pi/2$ and $\phi = 0$ we have, respectively,

$$V_{\pi,\pi/2} = \frac{f_\pi^2(r)}{2} \frac{\Omega^2}{D} \left[1 - \frac{\gamma^2}{2D} \right], \quad (70a)$$

$$V_{\pi,0} = \frac{f_\pi^2(r)}{2} \frac{\Omega^2}{D} \left[1 - \frac{(2\Delta - \delta)^2}{2D} \right], \quad (70b)$$

where D is given by Eq. (21).

In Fig. 14 we plot the variances of the out-of-phase $\phi = \pi/2$ (left panel) and in-phase $\phi = 0$ (right panel) quadratures. The interplay of parameters is a complex one, but we mostly use the ones of previous figures. For $\phi = \pi/2$ and $\Delta = 0$, as usual in resonance fluorescence systems, squeezing is restricted to a small range of Rabi frequencies, detunings, and Zeeman splittings. For $\phi = 0$ nonzero laser or Zeeman detunings are necessary to produce squeezing, with a strong dependence on their sign: on-resonance (not shown) there is no squeezing, as for a two-level atom; in Fig. 14(d) the laser is tuned below that transition, $\Delta = -2\gamma$, and there is no squeezing (positive variance) but the variance is reduced for large δ ; in Fig. 14(e) the laser is tuned above the transition, $\Delta = 2\gamma$, and there is squeezing for larger Rabi frequencies. Large values of δ tend to reduce the variance, be it positive or negative.

A. Out-of-phase quadrature

We now discuss a complementary view of the variance. For $\phi = \pi/2$ we can identify the Rabi frequency interval within which squeezing takes place,

$$0 < \Omega < \frac{1}{2} \sqrt{\gamma^2/2 - \delta^2/2 - 2(\Delta - \delta/2)^2}, \quad (71)$$

and the Rabi frequency for maximum squeezing is

$$\tilde{\Omega}_{\pi/2} = \frac{1}{2} \sqrt{\frac{\gamma^4/2 - 2[(\delta - \Delta)^2 + \Delta^2]^2}{3\gamma^2 + 2[(\delta - \Delta)^2 + \Delta^2]^2}}. \quad (72)$$

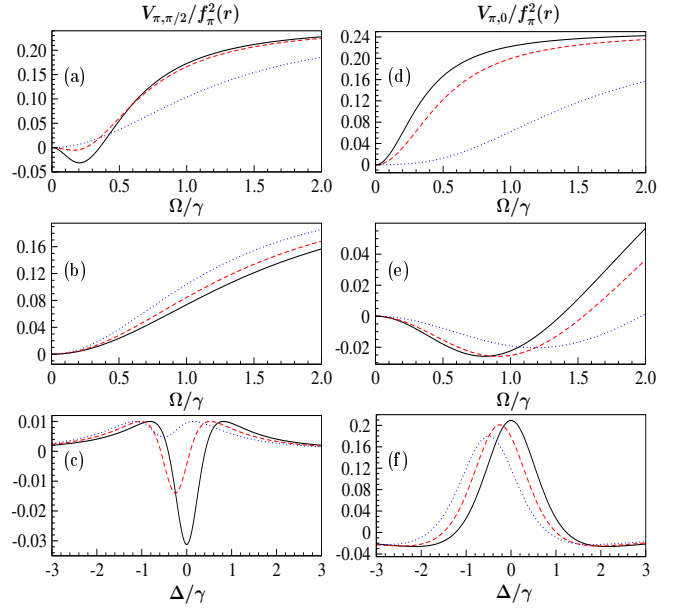


FIG. 14. Variance of the quadratures of the fluorescence of the π transitions: left panel for $\phi = \pi/2$ and right panel for $\phi = 0$. (a,b,d,e) as a function of Rabi frequency and (c,f) as a function of detuning. In all cases $\delta = 0$ is given by a solid-black line, and $\delta = -0.5\gamma$ by a dashed-red line; the dotted-blue line is $\delta = -2\gamma$ in (a,b,d,e) and $\delta = -\gamma$ in (c,f). Additionally, (a) $\Delta = 0$, (b) $\Delta = -2\gamma$, (c) $\Omega = 0.2\gamma$, (d) $\Delta = 0$, (e) $\Delta = 2\gamma$, (f) $\Omega = 0.8\gamma$.

Thus, the variance at $\tilde{\Omega}_{\pi/2}$ is

$$V_{\pi,\pi/2}^{(\tilde{\Omega}_{\pi/2})}(\Delta = 0, \delta) = \frac{f_\pi^2(r)}{16} \frac{(\gamma^4/2 - 2\delta^4)(\delta^2 - \gamma^2)}{\gamma^2(\gamma^2 + 2\delta^2)(\delta^2 + \gamma^2)}, \quad (73a)$$

for $\Delta = 0$ and $|\delta/\gamma| < 1/\sqrt{2}$;

$$V_{\pi,\pi/2}^{(\tilde{\Omega}_{\pi/2})}(\Delta, \delta = 0) = \frac{f_\pi^2(r)}{16} \frac{(\gamma^4/2 - 8\Delta^4)(4\Delta^2 - \gamma^2)}{\gamma^2(\gamma^2 + 4\Delta^2)^2}, \quad (73b)$$

for $\delta = 0$ and $|\Delta/\gamma| < 1/\sqrt{2}$; and the maximum total squeezing is obtained at $\Delta = \delta = 0$,

$$V_{\pi,\pi/2}^{(\tilde{\Omega}_{\pi/2})}(0, 0) = -\frac{f_\pi^2(r)}{32}, \quad \tilde{\Omega}_{\pi/2} = \frac{\gamma}{2\sqrt{6}}. \quad (73c)$$

For $\phi = \pi/2$ squeezing is limited to elliptical regions of weak driving and small detunings Δ and δ :

$$2\delta^2 + 8\Omega^2 < \gamma^2, \quad \Delta = 0, \quad (74a)$$

$$4\Delta^2 + 8\Omega^2 < \gamma^2, \quad \delta = 0. \quad (74b)$$

B. In-phase quadrature

For $\phi = 0$, squeezing is obtained in the Rabi frequency interval, for $\delta = 0$,

$$0 < \Omega < \frac{1}{\sqrt{2}} \sqrt{\Delta^2 - \gamma^2/4}, \quad |\Delta| > \gamma/2, \quad (75)$$

with maximum squeezing at the Rabi frequency

$$\tilde{\Omega}_0 = \frac{1}{2\sqrt{2}} \sqrt{\frac{16\Delta^2 - \gamma^2}{12\Delta^2 + \gamma^2}}, \quad (76)$$

requiring finite detuning from both π transitions ($\Delta \neq 0$) and stronger driving, $\Omega \sim \gamma$ [see Fig. 14(d)-(f)].

Thus, the variance at $\tilde{\Omega}_0$ is

$$V_{\pi,0}^{(\tilde{\Omega}_0)}(\delta) = -\frac{f_\pi^2(r)}{128} \frac{4\Delta^2 - \gamma^2}{\Delta^2(4\Delta^2 + \gamma^2)}, \quad |\Delta| \geq \gamma/2. \quad (77)$$

This expression gets the asymptotic value

$$\lim_{\Delta \rightarrow \infty} V_{\pi,0}^{(\tilde{\Omega}_0)} = -\frac{f_\pi^2(r)}{32}, \quad (78)$$

which is the same as that for the $\pi/2$ quadrature. The region for squeezing obeys the relation

$$4\Delta^2 - 8\Omega^2 < \gamma^2. \quad (79)$$

So, to obtain squeezing in this quadrature it is necessary to have detunings $\Delta > \gamma/4$ for any Rabi frequency.

IX. DISCUSSION AND CONCLUSIONS

We have studied several properties of the resonance fluorescence of the π transitions in a $J = 1/2 - J = 1/2$ angular momentum atomic system driven by a linearly polarized laser field and a magnetic field along the π transition to lift the level degeneracies. Interference among the various transition amplitudes create a rich landscape of effects. Most notable among our results is the observation of quantum beats when the atom is subject to large laser and magnetic fields. In this regime, two close Rabi frequencies interfere, giving rise to a well-defined modulation of the fast oscillations. These Rabi frequencies are the source of the two pairs of sidebands in the incoherent part of the power spectrum [5] and in the squeezing spectrum [10]. We studied beats in the total intensity and two-time functions such as the dipole-dipole, intensity-intensity and intensity-amplitude correlations. In the beats' regime the role of vacuum-induced coherence is small because the upper levels are very separated due to very large difference Zeeman splitting.

Before the beats we considered the previously overlooked time-dependent populations and reviewed aspects of the known stationary ones. The fact that the upper state populations evolve out of phase should not be a surprise. This, and nonzero initial population of both ground states (in contrast to nonzero populations of excited states for spontaneous emission), are major factors in the interference among the terms in the intensity. Except for very strong laser fields, the steady state populations depend strongly on the difference Zeeman splitting.

The AIC also permits to quantify the degree of non-Gaussianity; the fluctuations of third-order in the field quadrature amplitude due to strong atom-laser nonlinearity dominate over the second-order ones with strong

driving. The beats are in the strongly non-Gaussian regime.

The correlations show nonclassical features of the fluorescence light such as antibunching, $g^{(2)}(0) = 0$, and violation of classical inequalities in the amplitude-intensity correlations, Eqs. (61-62). We studied squeezing using the variance, i. e., the total noise in a quadrature, as well as using the second-order part of the spectrum. In the regime of beats there is squeezing, near the effective Rabi frequencies, but none in the total noise.

For a system with many parameters the interplay among them is a complex one, making the interpretation of results nontrivial. Thus, for most of our plots we chose parameters in two groups: i) where they are relatively small, $\Omega, \Delta, \delta \sim \gamma$, chosen to illustrate several degrees of vacuum-induced coherence; and ii) where they are large, $\Omega, \Delta, \delta \gg \gamma$, and quantum beats are revealed. Overall, particular care must be taken regarding detunings. On the one hand, large difference Zeeman splitting means that the excited levels would be very separated and interact with different frequency portions of the reservoir, hence diminishing the vacuum-induced coherence. On the other, large laser-atom detunings, which might increase the VIC, mean reduced fluorescence rates, which may also be detrimental in measurements. The beats, then, would be better observed if $\Delta \leq \gamma$ and δ of just several γ in the strong field regime.

X. ACKNOWLEDGMENTS.

The authors thank Dr. Ricardo Román-Ancheyta and Dr. Irán Ramos-Prieto for useful comments at an early stage of the project. ADAV thanks CONACYT, Mexico, for scholarship No. 804318.

ORCID numbers: Héctor M. Castro-Beltrán <https://orcid.org/0000-0002-3400-7652>, Octavio de los Santos-Sánchez <https://orcid.org/0000-0002-4316-0114>, Luis Gutiérrez <https://orcid.org/0000-0002-5144-4782>,

Appendix A: Time-Dependent Matrix Solutions and Spectra

The two-time photon correlations under study have the general form $\langle \mathbf{W}(\tau) \rangle = \langle O_1(0) \mathbf{R}(\tau) O_2(0) \rangle$, where \mathbf{R} is the Bloch vector and $O_{1,2}$ are system operators. The same applies to correlations of fluctuation operators $\Delta \mathbf{R}, \Delta O_{1,2}$. Using the quantum regression formula [30], the correlations obey the equation

$$\langle \dot{\mathbf{W}}(\tau) \rangle = \mathbf{M} \langle \mathbf{W}(\tau) \rangle, \quad (A1)$$

which has the formal solution

$$\langle \mathbf{W}(\tau) \rangle = e^{\mathbf{M}\tau} \langle \mathbf{W}(0) \rangle, \quad (A2)$$

where \mathbf{M} is given by

$$\mathbf{M} = \begin{pmatrix} -\gamma & -i\Omega & 0 & 0 & i\Omega & 0 & 0 & 0 \\ -i\Omega & -(\frac{\gamma}{2} + i\Delta) & 0 & 0 & 0 & i\Omega & 0 & 0 \\ 0 & 0 & -\gamma & i\Omega & 0 & 0 & -i\Omega & 0 \\ 0 & 0 & i\Omega & -(\frac{\gamma}{2} + i(\Delta - \delta)) & 0 & 0 & 0 & -i\Omega \\ i\Omega & 0 & 0 & 0 & -(\frac{\gamma}{2} - i\Delta) & -i\Omega & 0 & 0 \\ \gamma_1 & i\Omega & \gamma_\sigma & 0 & -i\Omega & 0 & 0 & 0 \\ 0 & 0 & -i\Omega & 0 & 0 & 0 & -(\frac{\gamma}{2} - i(\Delta - \delta)) & i\Omega \\ \gamma_\sigma & 0 & \gamma_2 & -i\Omega & 0 & 0 & i\Omega & 0 \end{pmatrix}. \quad (\text{A3})$$

Also, spectra of stationary systems can be evaluated more effectively using the above formal approach. Be $g(\tau) = \langle \mathbf{W}(\tau) \rangle$. Then, a spectrum is calculated as

$$\begin{aligned} S(\omega) &\propto \int_0^\infty \cos \omega \tau g(\tau) d\tau = \int_0^\infty \cos \omega \tau e^{\mathbf{M}\tau} g(0) d\tau \\ &= \text{Re} \int_0^\infty e^{-(i\omega \mathbf{1} - \mathbf{M})\tau} g(0) d\tau \\ &= \text{Re} [(i\omega \mathbf{1} - \mathbf{M})^{-1} g(0)], \end{aligned} \quad (\text{A4})$$

where $\mathbf{1}$ is the identity matrix. For example, the incoherent spectrum requires calculations of the type

$$\begin{aligned} S^{inc}(\omega) &= \text{Re} \int_0^\infty d\tau e^{-i\omega \tau} e^{\mathbf{M}\tau} \langle \Delta A_{ij}(0) \Delta A_{kl}(0) \rangle_{st} \\ &= \text{Re} [(\mathbf{M} - i\omega \mathbf{1})^{-1} \langle \Delta A_{ij}(0) \Delta A_{kl}(0) \rangle_{st}]. \end{aligned} \quad (\text{A5})$$

For the initial conditions of the correlations we use the following operator products and correlations in compact

form:

$$A_{kl} A_{mn} = A_{kn} \delta_{lm}, \quad (\text{A6a})$$

$$\langle A_{kl} A_{mn} \rangle = \alpha_{kn} \delta_{lm}, \quad (\text{A6b})$$

$$A_{ij} A_{kl} A_{mn} = A_{in} \delta_{jk} \delta_{lm}, \quad (\text{A6c})$$

$$\langle A_{ij} A_{kl} A_{mn} \rangle = \alpha_{in} \delta_{jk} \delta_{lm}. \quad (\text{A6d})$$

Hence, the relevant initial conditions are:

$$\langle A_{13} \mathbf{R} \rangle = (0, 0, 0, 0, \alpha_{11}, \alpha_{13}, 0, 0)^T, \quad (\text{A7a})$$

$$\langle A_{24} \mathbf{R} \rangle = (0, 0, 0, 0, 0, 0, \alpha_{22}, \alpha_{24})^T, \quad (\text{A7b})$$

$$\langle A_{13} \mathbf{R} A_{31} \rangle = (0, 0, 0, 0, 0, \alpha_{11}, 0, 0)^T, \quad (\text{A7c})$$

$$\langle A_{24} \mathbf{R} A_{42} \rangle = (0, 0, 0, 0, 0, 0, \alpha_{22})^T, \quad (\text{A7d})$$

$$\langle A_{13} \mathbf{R} A_{42} \rangle = \langle A_{24} \mathbf{R} A_{31} \rangle = 0, \quad (\text{A7e})$$

where $\mathbf{R} = (A_{11}, A_{13}, A_{22}, A_{24}, A_{31}, A_{33}, A_{42}, A_{44})^T$ is the Bloch vector. For correlations with fluctuation operator products, $\Delta A_{ij} = A_{ij} - \alpha_{ij}$, we have

$$\langle \Delta A_{kl} \Delta A_{mn} \rangle = \alpha_{kn} \delta_{lm} - \alpha_{kl} \alpha_{mn}, \quad (\text{A8})$$

$$\begin{aligned} \langle \Delta A_{ij} \Delta A_{kl} \Delta A_{mn} \rangle &= \alpha_{in} \delta_{lm} \delta_{jk} - \alpha_{il} \alpha_{mn} \delta_{jk} \\ &\quad - \alpha_{in} \alpha_{kl} \delta_{jm} - \alpha_{ij} \alpha_{kn} \delta_{lm} \\ &\quad + 2\alpha_{ij} \alpha_{kl} \alpha_{mn}. \end{aligned} \quad (\text{A9})$$

Now, recalling that $\alpha_{12} = \alpha_{14} = \alpha_{23} = \alpha_{34} = 0$, we write the detailed initial conditions of the correlations (Set 1 of Bloch equations and quantum regression formula):

$$\langle \Delta A_{13} \Delta \mathbf{R} \rangle = (-\alpha_{13} \alpha_{11}, -\alpha_{13}^2, -\alpha_{13} \alpha_{22}, -\alpha_{13} \alpha_{24}, \alpha_{11} - |\alpha_{13}|^2, \alpha_{13} - \alpha_{13} \alpha_{33}, -\alpha_{13} \alpha_{42}, -\alpha_{13} \alpha_{44})^T, \quad (\text{A10a})$$

$$\langle \Delta A_{24} \Delta \mathbf{R} \rangle = (-\alpha_{24} \alpha_{11}, -\alpha_{24} \alpha_{13}, -\alpha_{24} \alpha_{22}, -\alpha_{24}^2, -\alpha_{24} \alpha_{31}, -\alpha_{24} \alpha_{33}, \alpha_{22} - |\alpha_{24}|^2, \alpha_{24} - \alpha_{24} \alpha_{44})^T, \quad (\text{A10b})$$

$$\begin{aligned} \langle \Delta A_{13} \Delta \mathbf{R} \Delta A_{31} \rangle &= (2|\alpha_{13}|^2 \alpha_{11} - \alpha_{11}^2, 2|\alpha_{13}|^2 \alpha_{13} - 2\alpha_{11} \alpha_{13}, \\ &\quad 2|\alpha_{13}|^2 \alpha_{22} - \alpha_{11} \alpha_{22}, 2|\alpha_{13}|^2 \alpha_{24} - \alpha_{11} \alpha_{24}, \\ &\quad 2|\alpha_{13}|^2 \alpha_{31} - 2\alpha_{11} \alpha_{31}, 2|\alpha_{13}|^2 \alpha_{33} + \alpha_{11} - 2|\alpha_{13}|^2 - \alpha_{11} \alpha_{33}, \\ &\quad 2|\alpha_{13}|^2 \alpha_{42} - 2\alpha_{11} \alpha_{42}, 2|\alpha_{13}|^2 \alpha_{44} - \alpha_{11} \alpha_{44})^T. \end{aligned} \quad (\text{A10c})$$

$$\begin{aligned} \langle \Delta A_{24} \Delta \mathbf{R} \Delta A_{42} \rangle &= (2|\alpha_{24}|^2 \alpha_{11} - \alpha_{11} \alpha_{22}, 2|\alpha_{24}|^2 \alpha_{13} - \alpha_{22} \alpha_{13}, \\ &\quad 2|\alpha_{24}|^2 \alpha_{22} - \alpha_{22}^2, 2|\alpha_{24}|^2 \alpha_{24} - 2\alpha_{22} \alpha_{24}, \\ &\quad 2|\alpha_{24}|^2 \alpha_{31} - \alpha_{22} \alpha_{31}, 2|\alpha_{24}|^2 \alpha_{33} - \alpha_{22} \alpha_{33}, \\ &\quad 2|\alpha_{24}|^2 \alpha_{42} - 2\alpha_{22} \alpha_{42}, 2|\alpha_{24}|^2 \alpha_{44} + \alpha_{22} - 2|\alpha_{24}|^2 - \alpha_{22} \alpha_{44})^T. \end{aligned} \quad (\text{A10d})$$

$$\begin{aligned} \langle \Delta A_{13} \Delta \mathbf{R} \Delta A_{42} \rangle &= (2\alpha_{13}\alpha_{11}\alpha_{42}, 2\alpha_{13}^2\alpha_{42}, 2\alpha_{13}\alpha_{22}\alpha_{42}, (2|\alpha_{24}|^2 - \alpha_{22})\alpha_{13}, \\ &\quad (2|\alpha_{13}|^2 - \alpha_{11})\alpha_{42}, (2\alpha_{13}\alpha_{33} - \alpha_{13})\alpha_{42}, 2\alpha_{13}\alpha_{42}^2, (2\alpha_{13}\alpha_{44} - \alpha_{13})\alpha_{42})^T, \end{aligned} \quad (\text{A10e})$$

$$\begin{aligned} \langle \Delta A_{24} \Delta \mathbf{R} \Delta A_{31} \rangle &= (2\alpha_{24}\alpha_{11}\alpha_{31}, (2|\alpha_{13}|^2 - \alpha_{11})\alpha_{24}, 2\alpha_{24}\alpha_{22}\alpha_{31}, 2\alpha_{24}^2\alpha_{31}, \\ &\quad 2\alpha_{24}\alpha_{31}^2, (2\alpha_{24}\alpha_{33} - \alpha_{24})\alpha_{31}, (2|\alpha_{24}|^2 - \alpha_{22})\alpha_{31}, (2\alpha_{24}\alpha_{44} - \alpha_{24})\alpha_{31})^T. \end{aligned} \quad (\text{A10f})$$

Appendix B: Condition for Optimal Appearance of Beats in the Intensity

We consider a simplified, unitary, model to estimate the optimal initial population of the ground states to make well-formed beats. First, we diagonalize the Hamiltonian Eq. (8). The eigenvalues and eigenstates are

$$\mathcal{E}_1^\pm = -\frac{\Delta}{2} \pm \frac{1}{2}\sqrt{4\Omega^2 + \Delta^2}, \quad (\text{B1a})$$

$$\mathcal{E}_2^\pm = B_\ell + \frac{\delta - \Delta}{2} \pm \frac{1}{2}\sqrt{4\Omega^2 + (\delta - \Delta)^2}, \quad (\text{B1b})$$

and

$$\begin{aligned} |u_1\rangle &= \sin \Theta_1 |1\rangle + \cos \Theta_1 |3\rangle, \\ |u_2\rangle &= -\cos \Theta_1 |1\rangle + \sin \Theta_1 |3\rangle, \\ |u_3\rangle &= \sin \Theta_2 |2\rangle + \cos \Theta_2 |4\rangle, \\ |u_4\rangle &= -\cos \Theta_2 |2\rangle + \sin \Theta_2 |4\rangle, \end{aligned} \quad (\text{B2})$$

respectively, where

$$\begin{aligned} \sin \Theta_1 &= \frac{2\Omega}{\sqrt{(\Delta + \sqrt{\Delta^2 + 4\Omega^2})^2 + 4\Omega^2}}, \\ \cos \Theta_1 &= \frac{\Delta + \sqrt{\Delta^2 + 4\Omega^2}}{\sqrt{(\Delta + \sqrt{\Delta^2 + 4\Omega^2})^2 + 4\Omega^2}}, \\ \sin \Theta_2 &= \frac{2\Omega}{\sqrt{((\delta - \Delta) + \sqrt{(\delta - \Delta)^2 + 4\Omega^2})^2 + 4\Omega^2}}, \\ \cos \Theta_2 &= \frac{(\delta - \Delta) + \sqrt{(\delta - \Delta)^2 + 4\Omega^2}}{\sqrt{((\delta - \Delta) + \sqrt{(\delta - \Delta)^2 + 4\Omega^2})^2 + 4\Omega^2}}. \end{aligned} \quad (\text{B3})$$

It is now straightforward to obtain the excited-state populations. If the initial state of the system is $\rho(0) = \langle A_{33}(0) \rangle |3\rangle\langle 3| + \langle A_{44}(0) \rangle |4\rangle\langle 4|$ we get

$$\langle A_{33}(t) \rangle = \frac{1}{2} \langle A_{33}(0) \rangle \sin^2(2\Theta_1)(1 - \cos(\Omega_1 t)), \quad (\text{B4a})$$

$$\langle A_{44}(t) \rangle = \frac{1}{2} \langle A_{44}(0) \rangle \sin^2(2\Theta_2)(1 - \cos(\Omega_2 t)), \quad (\text{B4b})$$

and the intensity of the field is

$$\begin{aligned} \frac{I_\pi(\mathbf{r}, t)}{f_\pi^2(r)} &= \langle A_{33}(0) \rangle \sin^2(2\Theta_1) + \langle A_{44}(0) \rangle \sin^2(2\Theta_2) \\ &\quad - \langle A_{33}(0) \rangle \sin^2(2\Theta_1) \cos(\Omega_1 t) \\ &\quad - \langle A_{44}(0) \rangle \sin^2(2\Theta_2) \cos(\Omega_2 t). \end{aligned} \quad (\text{B5})$$

A necessary condition for the beating behavior to occur is that the initial ground-state populations are both nonvanishing in the nondegenerate case. Now, assuming the relation

$$\frac{\langle A_{33}(0) \rangle}{\langle A_{44}(0) \rangle} = \frac{\sin^2(2\Theta_2)}{\sin^2(2\Theta_1)} \quad (\text{B6})$$

is satisfied by choosing appropriate parameter values (Ω, δ, Δ) for given values of initial ground state populations we would get

$$\begin{aligned} I_\pi(\mathbf{r}, t) &= f_\pi^2(r) \langle A_{33}(0) \rangle \sin^2(2\Theta_1) \\ &\quad \times [1 - \cos(\Omega_{beat} t) \cos(\Omega_{av} t)], \end{aligned} \quad (\text{B7})$$

where $\Omega_{beat} = (\Omega_2 - \Omega_1)/2$ and $\Omega_{av} = (\Omega_2 + \Omega_1)/2$.

- [1] Z. Ficek and S. Swain, Phys. Rev. A **69**, 023401 (2004).
- [2] Z. Ficek and S. Swain, *Quantum Interference and Coherence: Theory and Experiments* (Springer, New York, 2005).
- [3] D. Polder and M. F. H. Schuurmans, Phys. Rev. A **14**, 1468 (1976).
- [4] M. Kiffner, J. Evers, and C. H. Keitel, Phys. Rev. Lett. **96**, 100403 (2006).
- [5] M. Kiffner, J. Evers, and C. H. Keitel, Phys. Rev. A **73**, 063814 (2006).

- [6] M. Kiffner, M. Macovei, J. Evers, and C. H. Keitel, in Progress in Optics, E. Wolf, ed. **55**, 85 (2010).
- [7] U. Eichmann, J. C. Bergquist, J. J. Bollinger, J. M. Gilligan, W. M. Itano, D. J. Wineland, and M. G. Raizen, Phys. Rev. Lett. **70**, 2359 (1993).
- [8] S. Das and G. S. Agarwal, Phys. Rev. A **77**, 033850 (2008).
- [9] H.-B. Zhang, S.-P. Wu, and G.-X. Li, Phys. Rev. A **102**, 053717 (2020).
- [10] H.-T. Tan, H.-X. Xia, and G.-X. Li, J. Phys. B: At. Mol.

- Opt. Phys., **42**, 125502 (2009).
- [11] M. Fischer, B. Srivathsan, L. Alber, M. Weber, M. Sonderman, and G. Leuchs, Appl. Phys. B: Lasers and Optics, **123**, 48 (2017).
 - [12] S. Wolf, S. Richter, J. von Zanthier, and F. Schmidt-Kaler, Phys. Rev. Lett. **124**, 063603 (2020).
 - [13] M. Jakob and J. Bergou, Phys. Rev. A **60**, 4179 (1999).
 - [14] H. B. Crispin and R. Arun, J. Phys. B: At. Mol. Opt. Phys., **52**, 075402 (2019).
 - [15] H. B. Crispin and R. Arun, J. Phys. B: At. Mol. Opt. Phys., **53**, 055402 (2020).
 - [16] R. Hanbury-Brown and R. Q. Twiss, Nature **177**, 27 (1956).
 - [17] R. J. Glauber, Phys. Rev. Lett. **10**, 84 (1963).
 - [18] H. J. Carmichael, H. M. Castro-Beltran, G. T. Foster, and L. A. Orozco, Phys. Rev. Lett. **85**, 1855 (2000).
 - [19] G. T. Foster, L. A. Orozco, H. M. Castro-Beltran, and H. J. Carmichael, Phys. Rev. Lett. **85**, 3149 (2000).
 - [20] L. Gutiérrez, H. M. Castro-Beltrán, R. Román-Ancheyta, and L. Horvath, J. Opt. Soc. Am. B **34**, 2301 (2017).
 - [21] G. S. Agarwal, *Quantum Statistical Theories of Spontaneous Emission and their Relation to Other Approaches* (Springer-Verlag, Berlin, 1974).
 - [22] B. R. Mollow, Phys. Rev. **188**, 1969 (1969).
 - [23] H. M. Castro-Beltrán, R. Román-Ancheyta, and L. Gutiérrez, Phys. Rev. A **93**, 033801 (2016).
 - [24] O. de los Santos-Sánchez and H. M. Castro-Beltrán, J. Phys. B: At. Mol. Opt. Phys. **54**, 055002 (2021).
 - [25] E. V. Shchukin and W. Vogel, Phys. Rev. A **72**, 043808 (2005).
 - [26] E. V. Shchukin and W. Vogel, Phys. Rev. Lett. **96**, 200403 (2006).
 - [27] Y.-X. Wang and A. A. Clerk, Phys. Rev. R **2**, 033196 (2020).
 - [28] Q. Xu, E. Greplova, B. Julsgaard, and K. Mølmer, Phys. Scripta, **90**, 128004 (2015).
 - [29] P. R. Rice and H. J. Carmichael, J. Opt. Soc. Am. B **5**, 1661 (1988).
 - [30] H. J. Carmichael, *Statistical Methods in Quantum Optics 1: Master Equations and Fokker-Planck Equations* (Springer-Verlag, Berlin, 2002).